DOI: 10.3390/pharmaceutics13122168

Photothermal nanofibers enable safe engineering of therapeutic cells

Ranhua Xiong[1,2 *], Dawei Hua[1, 2], Jelter Van Hoeck[2], Dominika Berdecka[2, 3], Laurens Léger[4], Stijn De Munter[5], Juan C. Fraire[2], Laurens Raes[2], Aranit Harizaj[2], Félix Sauvage[2], Glenn Goetgeluk[6], Melissa Pille[6], Jeffrey Aalders[4], Joke Belza[7], Thibaut Van Acker[7], Eduardo Bolea-Fernandez[7], Ting Si[8], Frank Vanhaecke[7], Winnok H. De Vos[3], Bart Vandekerckhove[6], Jolanda van Hengel[4], Koen Raemdonck[2], Chaobo Huang[1 *], Stefaan C. De Smedt[1, 2, 9 *], Kevin Braeckmans[2, 9 *]

[1]Joint Laboratory of Advanced Biomedical Materials (NFU-UGent), International Innovation for Center for Forest Chemicals and Materials, College of Chemical Engineering, Nanjing Forestry University (NFU), Nanjing 210037, P. R. China

[2]Laboratory of General Biochemistry and Physical Pharmacy, Faculty of Pharmaceutical Sciences, Ghent University, Ottergemsesteenweg 460, Ghent 9000, Belgium

[3]Laboratory of Cell Biology and Histology, Department of Veterinary Sciences, University of Antwerp, Antwerp, Belgium

[4]Department of Human Structure and Repair, Faculty of Medicine and Health Sciences, Ghent University, Corneel Heymanslaan 10, Ghent 9000, Belgium

[5]Department of Diagnostic Sciences and Cancer Research Institute Ghent (CRIG), Ghent University, 9000 Ghent, Belgium

[6]Department of Diagnostic Sciences, Faculty of Medicine and Health Sciences, Ghent University, Corneel Heymanslaan 10, Entrance 38, Ghent 9000, Belgium

[7]Department of Chemistry, Atomic & Mass Spectrometry- A&MS research unit, Ghent University, Krijgslaan 281 – S12, Ghent 9000, Belgium

[8]Department of Modern Mechanics, University of Science and Technology of China, Hefei 230026, China

[9]Center for Advanced Light Microscopy, Ghent University, Belgium

*Email: Kevin.Braeckmans@UGent.be, Stefaan.Desmedt@UGent.be, Chaobo.Huang@njfu.edu.cn, ranhua.xiong@njfu.edu.cn

Abstract

Nanoparticle-sensitized photoporation is an upcoming approach for intracellular delivery of biologics, combining high efficiency and throughput with excellent cell viability. However, as it relies on close contact between nanoparticles and cells, its translation towards clinical applications is hampered by safety and regulatory concerns. Here, we show that light-sensitive iron oxide nanoparticles (IONPs) embedded in biocompatible electrospun nanofibers induce membrane permeabilization by photothermal effects without direct cellular contact with IONPs. The photothermal nanofibers are successfully used to deliver effector molecules, including CRISPR/Cas9 ribonucleoprotein complexes and siRNA, in adherent and suspension cells, including embryonic stem cells and hard-to-transfect T-cells without affecting cell proliferation or phenotype. *In vivo* experiments furthermore demonstrate successful tumor regression in mice treated with CAR-T cells in which expression of PD1 is downregulated after nanofiber photoporation with siPD1. In conclusion, cell membrane permeabilization with photothermal nanofibers is a promising concept towards the safe and more efficient production of engineered cells for therapeutic applications, including stem cell or adoptive T cell therapy.

Introduction

Many biotechnological and biomedical applications depend on engineered cells, which requires intracellular delivery of macromolecules like DNA, RNA or proteins *in vitro* or *ex vivo*[1, 2, 3, 4]. In order to overcome the limitations of chemical transfection reagents or viral vectors[5, 6, 7, 8, 9], there has been a marked surge in the development of new and improved physical transfection techniques all aimed at achieving efficient cell transfections *in vitro* or *ex vivo* with as little cytotoxicity as possible[10, 11]. Of those, Nanoparticle (NP)-sensitized photoporation, or photoporation in short, is a particularly promising upcoming physical transfection method offering a unique combination of efficiency, safety and flexibility[12, 13, 14, 15, 16, 17, 18, 19]. However, when it comes to producing engineered cells for therapeutic applications, the use of photoporation is associated with safety and regulatory concerns due to the presence of NPs[20, 21, 22, 23, 24, 25]. It has been shown that after photoporation with AuNP a significant amount of Au remains associated with those cells even after rigorous washing[26], and we will show that the same holds true when using iron-oxide NPs. Therefore, from a regulatory point of view, cells engineered by NP-sensitized photoporation would be classified as a "long-term invasive medical device with medium exposure", for which extensive biocompatibility testing needs to be performed as indicated in red in **Supplementary Table 1.** In case photoporation could be performed without exposing cells to NPs, it would be classified as "a short-term non-invasive medical device with low exposure", for which only minimal biocompatibility testing is required as indicated in green in **Supplementary Table 1**.

As shown in **Fig. 1a**, here we propose a straightforward approach based on Photothermal Electrospun Nanofibers (PEN). By incorporating light-sensitive NPs within biocompatible electrospun nanofibers[27, 28], we hypothesized that photothermal effects can still be transferred to nearby cells as in traditional NP sensitized photoporation, but without direct contact between cells and NPs (top right panel in **Fig. 1a**).

In this study we first characterize the morphology, density and distribution of IONPs embedded in the electrospun nanofibers. Next, we show that both adherent and suspension cells can be safely and efficiently transfected with a range of macromolecules upon irradiation of PEN with nanosecond laser pulses. By performing elemental analysis via inductively coupled plasma – tandem mass spectrometry (ICP-MS/MS), we demonstrate the absence of IONP leakage into the cell medium or cells after laser irradiation. Numerical simulations on heat transfer from the embedded IONPs to the cell membrane allow to understand how the laser pulse fluence, IONP aggregation state and distribution within the nanofibers influence cell

membrane permeability. After demonstrating the possibility to use PEN photoporation to genetically engineer hard-to-transfect cells like embryonic stem cells and human T cells, PEN photoporation is used to transfect CAR-T cells with siPD1, leading to reduced expression of the PD1 receptor and enhancing their tumor killing capacity *in vivo*. Together it shows that PEN enables cell membrane permeabilization in a variety of cell types without contact to potentially toxic photothermal nanoparticles, thus paving the way towards the use of photoporation for safe and efficient production of gene modified cell therapies.

Synthesis and characterization of photothermal electrospun nanofibers.

Nanofibers were prepared from a mixture of PCL and IONPs dissolved at various weight percentages in a N, N-Dimethylformamide (DMF)/ Tetrahydrofuran (THF) solution. Fibers were collected on microscope glass slides as shown in **Supplementary Fig. 1a,b**. Scanning electron microscopy (SEM) and transmission electron microscopy (TEM) revealed an average fiber diameter of ~300 nm irrespective of the IONP concentration (**Fig. 1b-d**). By confocal microscopy it was found that the PEN web thickness gradually increased up to 4 µm after 1 h of electrospinning **Fig. 1e,f**). As the webs did not change much after 30 min, we selected this electrospinning time for all fiber webs created from here on. When adding increasing amounts of IONPs to the nanofibers, the PEN web's thickness did not change significantly (**Fig. 1g**).

Next, we analyzed how IONPs are distributed within the nanofibers. While IONPs were difficult to see by SEM when operated at 1.5 kV, they could be clearly seen when increasing the voltage to 20 kV (**Fig. 1h**). Thus, we found that the IONP density linearly increased from 1.7 to 192 clusters/1000 µm² for 0.02% to 5% IONPs (**Fig. 1i**). Two dimensionless size parameters allow to further understand the IONP distribution. The first is $\tilde{l}_1$ (**Fig. 1j**), defined as the ratio of the apparent IONP cluster size d_c over the average diameter of a single IONP d_s (162 ± 41 nm as quantified by TEM images, see **Supplementary Fig. 1c**). If $\tilde{l}_1 > 1$ IONPs are in a clustered state, examples of which are shown in **Fig. 1k**. For a PEN web with 1% IONPs, we observed that $\tilde{l}_1 \geq 2$ for more than 90% of IONPs clusters in the fibers, indicating that most of the IONPs are present in a clustered state. The second dimensionless size parameter is $\tilde{l}_2$ (**Fig. 1j**), defined as the ratio of the IONP cluster size d_c and the nanofiber diameter D. We found that >80% of the IONPs clusters occupied more than half of the nanofibers diameter. Examples are shown at the top of **Fig. 1l**. Finally, we analyzed the distance h that IONP clusters are below the fiber surface. If $h > 0$ nm, the cluster is below the fiber surface, if $h = 0$ nm the cluster surface coincides with the fiber surface, and if $h < 0$ nm, the cluster is sticking out of the fiber.

Examples are shown at the top of **Fig. 1m**. As 86% of the IONPs clusters were less than 40 nm away from the fiber surface, one can expect excellent heat transfer from the IONPs to the fiber surface which will be in contact with the cell membrane, as will be examined in detail further on. It is of note that, although there is a small fraction of IONPs sticking out of the fiber (~10%, $h < 0$ nm), they are still covered by a very thin layer of PCL polymer, as can be seen in high resolution TEM images (**Supplementary Fig. 1d).** We did not observe substantial differences for any of those three parameters when increasing the IONPs content from 1% to 5% (**Supplementary Fig. 1e**).

PEN photoporation enables safe and efficient intracellular delivery in adherent cells.

Intracellular delivery by PEN photoporation was initially tested on HeLa cells. Cell culture wells were prepared from PEN webs as illustrated in **Supplementary Fig. 2**. Fibers were coated with collagen to facilitate cell attachment (**Supplementary Fig. 3a)**, which substantially increased the cell density and cell area as compared to cells grown on bare PCL fibers (**Supplementary Fig. 3b, c**). Depending on the IONP content the average number of IONP clusters per cell ranged from 0.26 (0.02%) to 159 (5.0%) (**Supplementary Fig. 3d**). To test successful intracellular delivery by PEN photoporation, red fluorescently labelled dextran of 10 kDa (RD10) was added to the cells cultured in PEN wells. After scanning one time with the 7 ns pulsed laser beam, cells were washed and the Calcein AM viability stain was added to the cells. Exemplary confocal images are shown in **Supplementary Fig. 3e** showing increasing intracellular delivery of RD10 with increasing laser fluence. Quantification of confocal images revealed that increasing the laser fluence or IONPs content generally lead to more intracellular delivery, although cell toxicity gradually increased as well (**Fig. 2a**). We opted to continue working with 1% IONP PEN webs and a laser fluence of 0.08 J/cm² as this resulted in optimal delivery efficiency with the least amount of laser energy. Finally, as explained in detail in **Supplementary Note 1**, we found that, contrary to free IONPs (**Supplementary Fig. 4**), PEN substrates can be repeatedly laser-activated, leading to gradually enhanced delivery efficiency (**Supplementary Fig. 5, 6**). This proved to be most useful for the delivery of large macromolecules (**Supplementary Fig. 8**).

Efficient intracellular delivery in suspension cells by PEN photoporation.

Next we tested if PEN photoporation can be used to deliver compounds in suspension cells. For this we used Jurkat cells, which is an immortalized line of human T lymphocytes and a widely used model for hard-to-transfect primary human T cells. Cells were added in the

presence of 10 kDa FITC-dextran (FD10) to PEN culture wells and allowed to sediment on the fibers for 5 min (**Supplementary Fig. 8a**). Depending on the IONP content, the number of IONP per cell ranged from 7.7 to 28.4 IONPs/cell (**Supplementary Fig. 8b**). Initial delivery experiments showed that positively charged nanofibers produced the best results rather than collagen coated ones (**Supplementary Fig. 8c**). From image analysis it was determined that the delivery efficiency increased with increasing laser fluence or IONP content at the expense of cell viability as measured by the calcein red-orange AM viability stain (**Fig. 2b**). If we set a threshold of minimal 80% viability, the best transfection efficiency (~75% positive cells) was obtained for a PEN substrate with 2% IONPs (~12 IONPs/cell, **Supplementary Fig. 8**) and a laser fluence of 0.16 J/cm². Finally, we again tested repeated PEN photoporation (bottom left panel **Fig. 1b**), finding that the percentage of positive cells could be increased by repeating the procedure with only little effect on cell viability. Note that for this experiment we used a PEN substrate with 2% IONPs with a suboptimal laser fluence of 0.08 J/cm² to better show the gradual improvement.

ICP-MS/MS confirms there is no leakage of IONPs from PEN substrates upon laser irradiation.

A crucial premise in this work was to avoid direct contact between sensitizing NPs and cells during photoporation. To verify whether condition is met, the cellular iron concentrations were determined using ICP-MS/MS (tandem ICP-mass spectrometry) after PEN photoporation. HeLa and Jurkat cells were photoporated using PEN substrates containing 1% or 2% IONPs, respectively. Next, as schematically shown in **Fig. 2c**, the cells were detached from the nanofibers and digested with *aqua regia* (3:1 mixture of hydrochloric acid and nitric acid) prior to ICP-MS/MS analysis. As a positive control, we included cells incubated with 500 µg/mL of 30 nm IONPs coated with polyethylene glycol for 4 h at 37 °C. As shown in **Fig. 2d**, the positive control indeed had a significantly higher iron concentration in comparison with the negative control (untreated cells) for both cell types. Importantly, however, the iron content in PEN photoporated cells did not differ significantly from untreated cells irrespective of the laser fluence or number of laser scans. While this proves that there is no measurable increase in iron content in cells, one could argue that the endogenous iron content in cells is already fairly high so that small increases may not be easily detected. Therefore, we proceeded with measuring potential iron release from the PEN substrates when submerged in pure DI water (without any cells present, **Fig. 2e**). The iron content in DI water after laser activation of the PEN substrates did not significantly increase and remained below the detection limit of 0.08 mg/L irrespective of the IONP content, number of scans or laser fluence (**Fig. 2f**). Instead,

when IONP were intentionally released by digestion of PEN fibers with *aqua regia*, very high iron concentrations proportional to the embedded IONPs content (1, 2 or 5% IONPs) were indeed measured. All together we it can be concluded that IONP are not released from PEN substrates upon laser activation, thus avoiding any direct exposure of cells to potentially toxic sensitizing NPs or its constituents. Detailed numerical simulations show that efficient cell permeabilization is nevertheless possible by the fact that IONPs are close to the fiber surface, allowing efficient heat transfer towards distinct places of the cell membrane where pores are formed (**Supplementary Note 2,** and **Supplementary Figure 9-13**).

Efficient gene silencing or knockout in adherent cells by PEN photoporation.

After successful delivery of model macromolecules, we went on to test delivery of siRNA as a functional macromolecule, starting by delivering anti-GFP siRNA into adherent H1299 cells which stably express green fluorescence protein (GFP). As illustrated in **Fig. 3a**, cells were grown on collagen-coated PEN webs (1% IONPs) at 37°C for 24 h, after which they were PEN photoporated (0.08 J/cm²) with control and anti-GFP siRNA. Confocal microscopy confirmed qualitatively successful siRNA knockdown after 24 h when using 5 µM siRNA (**Fig. 3b**), which was confirmed quantitatively by flow cytometry (**Fig. 3c**). Knockdown efficiency increased with siRNA concentration (0.5, 1, 2 and 5 µM) without affecting cell viability, here measured by the cell Titer-Glo luminescent assay (**Fig. 3d-f**). Keeping the siRNA concentration fixed (0.5 µM), repeated laser scanning improved knockdown efficiency as well, reaching up to 70% after 4 laser scans, which is similar to a single scan with 5 µM siRNA.

We next investigated the delivery of CRISP-Cas9 ribonucleoproteins (RNPs). After PEN photoporation of H1299 cells with 0.5-4 µM RNPs, cells were allowed to grow for another 48 h before analysis. Exemplary confocal images and flow cytometry histograms are shown in **Fig. 3g, h**, respectively, confirming successful GFP knockout. GFP knockout efficiency increased along with the RNP concentration (**Fig. 3i, j**), reaching a knockout efficiency as high as 80% for the highest RNP concentration. Keeping the RNP concentration fixed (0.5 µM), repeated PEN photoporation (N=2, 3, 4) resulted in enhanced knockout efficiency. Together this shows that PEN photoporation is not only able to deliver relatively small biological molecules like siRNA, but also quite large macromolecular complexes like RNPs.

PEN photoporation achieves CIRSPR/Cas9 mediated gene knockouts in human embryonic stem cells without affecting cell functionality.

Next, we turned to human pluripotent stem cells which are relevant for stem cell therapy[29]. Human embryonic stem cells (hESCs) were grown on PEN nanofibers (1% IONP) modified with a Geltrex coating in order to facilitate their attachment and growth. After 3-4 days, the hESCs were PEN photoporated with RD10 (0.5 mg/mL) to investigate delivery efficiency. Quantification of confocal images revealed a gradual increase of delivery efficiency with a concomitant decrease of cell viability, here determined by live/dead staining. When calculating the delivery yield, which is the percentage of living and transfected cells compared to the initial number of cells, a maximum delivery yield of 61% was obtained for I=0.08 J/cm^2, which further increased to 71% if laser scanning was performed twice (N=2) (**Fig. 4a**). As a comparison we also delivered RD10 in hESCs by electroporation as an often-used non-viral transfection method for stem cells. With electroporation a delivery yield of only 53% was obtained for the best functioning electroporation program (CE-118) (**Fig. 4b**). Exemplary confocal images are shown in **Fig. 4c** of control hESCs as well as PEN photoporated and electroporated hESCs for the most optimal conditions. 24 h post treatment the difference was even more pronounced, with a cell yield of 63% for PEN photoporation and 25% for electroporation (**Fig. 4d**). This reduction in delivery yield for electroporation was due to a drop in viability from 72% after 2 h to only 34% after 24 h, pointing at long-term adverse effects in electroporated hESCs. To further investigate this, we compared the proliferation of electroporated and PEN photoporated hESCs. PEN photoporated cells were able to immediately recover and grow exponentially just like the untreated cells. Instead, it took the electroporated cells four days to recover and resume exponential growth (**Fig. 4e**).

Having established that PEN photoporation does not seem to have a great impact on hESC viability and proliferative capacity, next we examined pluripotency transcription factors Oct4 (Pou5f1), Sox2 and Nanog which are crucial for maintaining a pluripotent cell identity. Since we are interested in investigating the effect of the permeabilization method itself, these experiments were performed according to optimized conditions but in the absence of any cargo. Based on immunostaining and confocal images, PEN photoporated cells did not show any significant differences in comparison with non-treated hESCs (**Fig. 4f, g**). Furthermore, we differentiation potential of PEN photoporated hESC towards cardiomyocytes was unaltered compared to control cells based on immunostaining of the cardiomyocyte-specific markers TNNT2 and NKX2.5 (**Fig. 4h, i**). This is expected to be beneficial for downstream applications like differentiation to hESC-derived cardiomyocytes and subsequent transplantation[30].

Finally, we applied PEN photoporation to the intracellular delivery of CRISPR/Cas9 RNPs in hESCs in order to knockout the IL-2Rgamma (IL-2R) gene on the X chromosome, which is involved in X-linked severe combined immunodeficiency[31]. Sanger sequencing of PEN-photoporated hESCs with 2 µM RNPs revealed a knockout efficiency >60%, demonstrating successful CRISPR/Cas9 mediated gene knockout in difficult to transfect human embryonic stem cells (**Fig. 4j, k**).

PEN photoporation achieves efficient gene knockdown by siRNA delivery in primary human T cells.

Next, we applied PEN photoporation to human donor-derived T cells (**Supplementary Fig. 14**). First, PEN photoporation conditions were optimized by FD10 delivery. Using neutral PEN fibers, an IONP content of 5% was proven optimal with a laser fluence of 0.16 J/cm^2 (**Supplementary Fig. 15**). Using these optimized settings, a direct comparison was made between neutral and hydrated nanofibers which received a treatment with sodium hydroxide to increase their hydrophilicity and enhance cell adhesion[32]. Hydrated nanofibers produced the best results with a yield of 40.7% viable transfected cells with three times laser scanning (**Fig. 5a**). A comparison was performed with electroporation as the most commonly used non-viral transfection tool for nucleic acid delivery in T cells. Based on the manufacturer's recommendation, several protocols were tried (EO-100, EO-115, FI-115). With a viability of 26.2% and a delivery efficiency of 76.0%, the electroporation protocol EO-100 resulted in the highest FD10 delivery yield (19.3%) (**Fig. 5b**). While such low cell viability after electroporation may seem surprising considering the manufacturer's claim that >70% T-cell viability is expected for the EO-100 program, it should be noted that this is based on cell viability as measured by live/dead staining and quantification by flow cytometry, which leads to an overestimation of cell viability (**Supplementary Note 3,** and **Supplementary Fig. 16**).

Next, we applied the optimized PEN photoporation and electroporation protocols to deliver siRNA into human T cells to silence expression of the PD1 receptor. PD1 expression is typically upregulated in stimulated T cells and is considered an important mediator of T cell immunosuppression in the tumor micro-environment[33]. Human T cells were cultured for 7 days, transfected by PEN photoporation or electroporation according to the previously optimized conditions and stimulated with CD3/CD28 tetrameric antibody complexes and IL-2 to upregulate PD1 expression. From several tested siRNA constructs (**Supplementary table 2**), the D2 siRNA construct was found to perform best (**Supplementary Fig. 17**) and was selected for further optimization of PD1 gene silencing. PD1 expression could be silenced in human T cells both by photoporation and electroporation. Silencing became more effective as the

siPD1 concentration increased, reaching ~80% knockdown for 4 µM siPD1 with both PEN photoporation and electroporation (**Fig. 5c, d**). This shows that PEN photoporation cannot only achieve more living and transfected cells, but also results in a level of downregulation per cell that is similar to electroporation.

PEN photoporation does not alter T cell homeostasis and functionality *in vitro*, contrary to electroporation.

An optimal intracellular delivery technology should minimally disturb the cell's normal functioning and homeostasis, especially when applied to therapeutic cells[34, 35]. Therefore, we compared the downstream effects of PEN photoporation and electroporation on T cell morphology, phenotype and activation state (**Fig. 5e**-**h**). Human donor-derived T cells were subjected to PEN photoporation and electroporation in the absence of cargo so as to investigate the effects induced by the delivery technology itself. First of all, it was noted that electroporated cells had decreased in size 1 h after treatment, which was not the case for photoporated cells (**Fig. 5e**). This morphological change after electroporation was accompanied by a strong sustained increase in Ca^{2+} levels up to 6 h after treatment, which returned to baseline after 24 h (**Fig. 5f**). Instead, Ca^{2+} levels remained unaltered for PEN photoporated cells at all times.

Next, we studied production of inflammatory cytokines (TNFα, IFNγ, IL-5, IL-6, IL-9, IL-10, IL-13 and IL-17A) 24 h and 48 h after treatment. In response to PEN photoporation no significant increase of any of the cytokines was observed (**Fig. 5g**). In contrast, electroporation caused a significant upregulation of most inflammatory cytokines after 48 h (TNFα: 7.2-fold increase, IFNγ: 7.4-fold increase, IL-6: 2.9-fold increase, IL-9: 6.3-fold increase, IL-13: 3.0-fold increase and IL-17A: 4.7-fold increase, compared to non-treated T cells). We continued investigating the extent of upregulation of several activation markers, including CD137 (4-1BB), CD154 (CD40L) and PD-1. All of them were significantly upregulated 24 h and 48 h post electroporation, which was not the case for PEN photoporation except for a slight increase of PD-1 after 48h (**Fig. 5h)**. Together these results point at phenotypic changes caused by electroporation, which were absent in PEN photoporation-treated T cells.

Next, we validated the functionality of T cells after PEN photoporation and electroporation *in vitro*. T cell proliferation was investigated first, for which human T cells were PEN photoporated or electroporated (without cargo), followed by stimulation with CD3/CD28 beads. After electroporation, cell numbers decreased during the first 48 h, but started proliferate again after 72 h. This 2-3 day delay in proliferation post electroporation points to an anergic state (**Fig. 5i**). Interestingly, PEN photoporation fully preserved the proliferative

potential of the human T cells without any significant delay in growth compared to untreated T cells.

Finally, we compared the cytolytic capacity of electroporated and PEN photoporated T-cells previously transduced with a tumor-targeting chimeric antibody receptor (CAR T cells). The tumor-killing capacity of these CD70-targeted CAR T cells was evaluated *in vitro* on SKOV3 and H1650 cancer cell lines positive for CD70 antigen and expressing the PD1 ligand (PD-L1) at various levels (**Supplementary Fig. 18**). PEN photoporated cells demonstrated efficient tumor cell killing similar to untreated CAR T cells especially for a high effector to target ratio (**Fig. 5j**). However, electroporation clearly diminished the cytolytic capacity of CAR T cells. Taken together, these results confirm the presence of an anergic state in electroporated cells, which is a consequence of the long-term adverse effects on T cell homeostasis, as was also reported before[34]. In strong contrast, PEN photoporated T cells do not suffer from altered homeostasis and fully retain their cytolytic functionality.

CAR-T cells transfected with siPD1 by PEN photoporation offer therapeutic functionality *in vivo*.

Having confirmed that PEN photoporation does not negatively affect T cell fitness nor the cytolytic potential of CAR T cells, we finally evaluated their efficacy *in vivo* in a SKOV3 tumor mouse model (**Fig. 6a**). We found that CAR T cells alone, CAR T cells PEN photoporated with siPD1 and CAR T cells combined with injection of PD1-antibodies can control the tumor growth in a period of one month (**Fig. 6b** and **Supplementary Fig. 19**). Most importantly, we observed that siPD1 treated CAR T cells were able to significantly reduce the tumor volume after already 21 days, which was identical to the positive control with PD-1 antibodies (**Fig. 6b**). Instead, it took 25 days for CAR T cells alone to significantly control the tumor volume. These in vivo data confirm that PEN photoporated T cells fully retain their therapeutic potential and that siRNA mediated knockdown of the PD-1 receptor can provide a therapeutic advantage for the treatment of solid tumors.

Conclusions

In summary, we have developed a methodology for the intracellular delivery of macromolecules which keeps the key beneficial features of NP-sensitized photoporation but without direct exposure of cells to the sensitizing NPs. We have shown that it can efficiently induce gene knockout in stem cells and gene silencing in primary human T-cells, showing that PEN photoporation has potential for clinical translation such as for the generation of engineered cells for cell therapies, including stem cell therapy or adoptive T cell therapy.

Acknowledgements

This research was supported by National Natural Science Foundation of China (No. 21774060, 21644004), European Research Council (ERC Consolidator Grant, 648124), the Research Foundation Flanders (FWO, 1500418N, 12Q8718N and 1S62517N), the National Key R&D Program of China (2017YFF0207804), and the Youth Innovation Promotion Association CAS (No. 2018491). The authors would like to acknowledge funding from the European Union's Horizon 2020 research and innovation programme under grant agreement No 810685 (DelNam project).

Author Contributions

RX, KB and SDS conceived the concept of PEN photoporation for contact-free photoporation and designed the experiments. RX, CH and DH fabricated and characterized the PEN substrates. RX performed the PEN photoporation experiments with data analysis, and performed CFD simulations together with JF. JB, EBF and TVA performed and analyzed the ICP-MS measurements. LR and MP prepared the RNPs. LL and JA were involved in the preparation and PEN photoporation of hESCs. JVH, DB, SDM, KR, GG, AH, FS and BV were involved in the preparation and PEN photoporation of human T cells. KB, SDS, CH, KR, TS, FV, JVH, WDV and BV advised on experiments and data analysis. All authors discussed the experimental results and jointly wrote the manuscript.

Competing Interests

The authors declare no competing financial interests.

Figure Captions

Figure 1. Concept of intracellular delivery by photothermal nanofibers and characterization of photothermal electrospun nanofibers. (**a**) Schematic overview of intracellular delivery by membrane permeabilization with photothermal nanofibers. (**b**) SEM and TEM images of electrospun polycaprolactone nanofibers containing 0 and 1 wt% IONPs. Scale bars in the left image are 2 μm and the right are 1 μm. (**c**) Histogram of the nanofiber's diameter without IONPs, based on the analysis of 536 individual nanofibers. (**d**) Nanofiber diameter for increasing IONPs content (0 - 5%) determined from electron microscopy images (n=469, 275, 413, 536, 423 and 417, median value, the box from the 25^{th} to 75^{th}, percentile with whiskers from the 5^{th} to the 95^{th}). (**e**) Confocal microscope images of nanofibers (without IONPs) shown in 3D, as a z-projection and an exemplary horizontal section (Scale bar 20 μm). (**f**) For increasing electrospinning time, the fiber web's total thickness was measured from 3D confocal z-stacks (n=9 images obtained from three samples, mean ± SD). (**g**) The total thickness of nanofiber webs was measured for increasing IONPs content after 30 min electrospinning time (n=3 independent samples, mean ± SD). (**h**) SEM imaging at 20 kV clearly reveals IONPs within the fibers (bottom), which was not the case at a lower voltage of 1.5 kV (top, Scale bar 300 nm). (**i**) The density of IONPs clusters was quantified by per unit area in the SEM images (Scale bar 2 μm) (for each condition n=10 images were recorded from three PEN samples). (**j**) Schematic drawing illustrating three parameters that were used to describe the distribution of IONPs within the nanofibers. (**k**) The dimensionless size $\tilde{l}_1$ quantifies the extent to which IONPs are clustered in nanofibers. The TEM images at the top illustrate three different clusterization states of IONPs embedded in nanofibers. The histogram of the dimensionless size $\tilde{l}_1$ is shown at the bottom (n=128). (**l**) Similar images and a histogram are shown for the dimensionless parameter $\tilde{l}_2$ which expresses the size of the clusters relative to the fiber diameter (n=128). (**m**) Similar images and a histogram are shown for the parameter *h* which is the distance between the IONPs cluster's outer surface and the fiber surface (n=128 clusters in three PEN samples).

Figure 2. PEN photoporation efficiently and repeatedly delivers macromolecules to adherent and suspension cells with minimal toxicity and without potential IONPs leakage from laser-activated PEN substrates. (**a**) Delivery efficiency of red fluorescently labelled 10 kDa dextran (RD10) and cell viability (Calcein positive cells) were quantify as a function of laser pulse fluence for PEN webs with different amounts of IONPs: 0.02%, 0.1%, 1.0% and 2.0%. (n=3, independent experiments, mean ± SD) (**b**) Jurkat cell viability and delivery efficiency of RD10 shown as function of laser fluence and IONPs content of 1.0%, 2.0% and 5.0%; and cell viability and delivery efficiency of FD10 in Jurkat cells for repeated PEN photoporation using 2% IONPs and I=0.08 J/cm^2. (n=3, independent experiments, mean ± SD) (**c**) Schematic overview of the experimental procedure to determine the iron content in cells by ICP-MS/MS after PEN photoporation. (**d**) The iron concentration was measured in untreated cells (negative control), cells incubated with IONPs with or without laser scanning (positive controls), and cells treated by PEN photoporation. For HeLa cells PEN substrates with 1% IONPs were used, while it was 2% for Jurkat cells. Laser fluences were varied from 0.08 to 0.16 J/cm², with repeated photoporation from N=1 to 4 times. (n=4 independent experiments, mean ± SD, *P=0.015, ***P=1.972 X 10^{-4}, **P=0.0018, **P=0.0014 from left to right, one-way ANOVA). (**e**) Schematic overview of the experimental procedure to measure potential iron leakage from laser-activated PEN substrates into DI water. (**f**) The iron concentration was determined by ICP-MS/MS in DI water (negative control), in *aqua regia* in which an amount of fibers comparable to one PEN culture well with IONPs content of 1%, 2% or 5% (positive control) were digested, and in DI water collected from the PEN substrates after laser activation. PEN substrates with 1 and 5% IONPs were tested, without and with N=1 and 4 times laser activation at a laser fluence of 0.08 and 0.16 J/cm². (n=3, independent experiments, mean ± SD)

Figure 3. PEN photoporation for siRNA gene silencing or CRISPR/Cas9 mediated gene knockout in H1299. (a) Schematic overview of the experimental procedure to deliver siRNA or RNPs into GFP expressing H1299 cells by PEN photoporation. (**b**) Confocal images showing GFP expressing H1299 cells PEN photoporated with 5 μM control (left) and anti-GFP siRNA (right). PEN substrates contained 1% IONPs and were 1x scanned with a laser fluence of 0.08 J/cm^2. (**c**) The corresponding flow cytometry histograms show how GFP expression is distributed over the cell population when PEN photoporated with control or anti-GFP siRNA. (**d-e**) H1299 cells were on the one hand 1x PEN photoporated with increasing concentrations of siRNA (0.5, 1, 2, 5 μM), and on the other hand multiple times (N=2, 3, 4). The MFI (**d**) and knockdown efficiency (**e**) were quantified by flow cytometry (n=3, independent experiments, mean ± SD). (**f**) The corresponding cell viability is shown as measured by the Cell Titer Glo assay. (**g**) Exemplary confocal images showing eGFP expression in H1299 cells before and 48 h after PEN photoporation with 4 μM RNPs targeted to the eGFP gene (I=0.08 J/cm², 1% IONPs). Scale bars are 200 μm. (**h**) Corresponding flow cytometry histograms. (**i-j**) H1299 cells were either 1x PEN photoporated (I = 0.08 J/cm²) with increasing concentrations of RNPs (0.5, 1, 2, 4 μM), or multiple times (N=2, 3, 4) for a RNP concentration of 0.5 μM. The MFI (**i**) and knockout efficiency (**j**) were measured by flow cytometry (n=3, independent experiments, mean ± SD).

Figure 4. PEN photoporation enables efficient intracellular delivery of macromolecules, including CRISPR/Cas9 ribonucleoprotein complexes, in human embryonic stem cells (hESC) without affecting cell functionality. (**a**) Delivery efficiency, cell viability and the delivery yield were quantified 2 h after PEN photoporation as a function of laser pulse fluence (I = 0.04, 0.08, 0.12 and 0.24 J/cm²) and repeated PEN photoporation (N = 2, 4; I=0.08 J/cm²) (n=3, independent experiments, mean ± SD). (**b**) Delivery efficiency, cell viability and the delivery yield for different hESC electroporation programs measured 2 h after treatment. (**c**) Confocal images show green fluorescence from Calcein-AM viability staining, red fluorescence from PI positive dead cells and magenta from RD10 (Scale bar 50 μm). (**d**) The viability and yield were measured 24 h after treatment with PEN photoporation or electroporation using the most optimal protocols (I=0.08 J/cm^2, N=2 for PEN photoporation and the CE-118 program for electroporation). (**e**) Cell proliferation post PEN photoporation and electroporation using the most optimal protocols (n=3, independent experiments, mean ± SD). (**f**) Confocal images of hESCs immunostained for pluripotency transcription factors Oct4 (Pou5f1), Sox2 and Nanog 24 h after PEN photoporation. Nuclei are stained by Hoechst (Scale bar 50 μm). (**g**) Expression of Oct4 (Pou5f1), Sox2 and Nanog relative to untreated cells as quantified from confocal images (n=3, independent experiments, mean ± SD). (**h**) Confocal images of hESCs differentiated into cardiomyocytes and immunostained for the cardiomyocyte-specific markers TNNT2 and NKX2.5. (**i**) Expression of TNNT2 and NKX2.5 relative to untreated cells as quantified from confocal images (Scale bar 200 μm) (n=3, independent experiments, mean ± SD). (**j**) Sanger sequences of non-treated hESCs (NTC), hESCs PEN photoporated without RNP (PEN Ctrl), hESCs PEN photoporated with 2 μM mock RNPs (RNP Ctrl) and hESCs PEN photoporated with 2 μM IL-2R RNPs (IL-2R RNP). (**k**) IL-2R knockout efficiency by Sanger sequencing and tracking of indels by decomposition (TIDE) analysis. All analyzed results have a model fit R^2>0.9, which indicates how well the indel distribution fits the sanger sequencing data (ICE v2 analysis by Synthego) (n=3, independent experiments, mean ± SD).

Figure 5. PEN photoporation enables efficient intracellular delivery of siRNA in human donor derived T cells with minimal toxicity, optimal T cell fitness, and retaining T cell effector functions *in vitro*. (**a**) FD10 delivery efficiency, viability and delivery yield in human T cells photoporated with hydrated or neutral PEN nanofibers. NTC = nontreated control. (**b**) Screening of different electroporation programs for optimal FD10 delivery efficiency, viability and yield. (**c**) Exemplary histograms showing PD1 expression in CD3+ T cells 48 h after PEN photoporation of T cells with 4 µM siPD1. (**d**) Optimization of PD1 silencing as a function of siPD1 concentration using the optimized PEN photoporation and electroporation delivery protocols. (**e**) Impact on cell size 1 hour post-treatment. Values are expressed relative (%) to NTC. (**f**) Calcium levels of nontreated cells compared to PEN photoporated or electroporated T cells 1 h, 6 h and 24 h post-treatment. Values are expressed relative to the nontreated control. (**g**) Secretion of several key pro-inflammatory and anti-inflammatory cytokines was measured in the supernatant of human T cells, 24 h or 48 h after electroporation or PEN photoporation. (**h**) Expression levels of activation markers CD137 and CD154, as well as activation/exhaustion marker PD1 were measured 24 h and 48 h after treatment with electroporation or PEN photoporation compared to the nontreated control (relative fold change). (**i**) Proliferation of PEN photoporated or electroporated T cells (without cargo molecules) was measured up to 72 h after stimulation with CD3/CD28 tetrameric antibody complexes in the presence of IL-2. (**j**) Cytolytic activity was measured with a standard 4 h chromium-51 release assay. Statistical significance relative to NTC is indicated when appropriate. (n=3, biologically independent samples, mean ± SD, one-way ANOVA)

Figure 6. PEN photoporation retains as well T cell effector functions *in vivo*. (**a**) Schematic overview of the experimental procedure to deliver siRNA into previously transduced CAR T cells by PEN photoporation to demonstrate efficacy in a SKOV3 tumor mouse model. (**b**) The tumor size was monitored over time for mice intravenously injected with CAR T cells (n=5 mice), CAR T cells PEN photoporated with siPD1 (n=4 mice), or CAR T cells combined with PD1-antibody administration (positive control, n=4 mice). Control mice were treated with PBS alone (n=4 mice). Statistical significance relative to NTC is indicated when appropriate. (mean ± SD, one-way ANOVA)

References

1. Lee J, Bayarsaikhan D, Bayarsaikhan G, Kim J-S, Schwarzbach E, Lee B. Recent advances in genome editing of stem cells for drug discovery and therapeutic application. *Pharmacology & Therapeutics* 2020, **209:** 107501.

2. Vodnala SK, Eil R, Kishton RJ, Sukumar M, Yamamoto TN, Ha N-H*, et al.* T cell stemness and dysfunction in tumors are triggered by a common mechanism. *Science* 2019, **363**(6434)**:** eaau0135.

3. Cox DBT, Platt RJ, Zhang F. Therapeutic genome editing: prospects and challenges. *Nat Med* 2015, **21**(2)**:** 121-131.

4. Zhou PH, Shaffer DR, Arias DAA, Nakazaki Y, Pos W, Torres AJ*, et al.* In vivo discovery of immunotherapy targets in the tumour microenvironment. *Nature* 2014, **506**(7486)**:** 52-+.

5. McManus MT, Haines BB, Dillon CP, Whitehurst CE, van Parijs L, Chen J*, et al.* Small Interfering RNA-Mediated Gene Silencing in T Lymphocytes. *The Journal of Immunology* 2002, **169**(10)**:** 5754.

6. June CH, Blazar BR, Riley JL. Engineering lymphocyte subsets: tools, trials and tribulations. *Nature Reviews Immunology* 2009, **9**(10)**:** 704-716.

7. Peer D. A daunting task: manipulating leukocyte function with RNAi. *Immunological reviews* 2013, **253:** 185-197.

8. Yin H, Kanasty RL, Eltoukhy AA, Vegas AJ, Dorkin JR, Anderson DG. Non-viral vectors for gene-based therapy. *Nature reviews Genetics* 2014, **15**(8)**:** 541-555.

9. Kaiser J. Gene therapy trials for sickle cell disease halted after two patients develop cancer. *Science* 2021.

10. Stewart MP, Langer R, Jensen KF. Intracellular Delivery by Membrane Disruption: Mechanisms, Strategies, and Concepts. *Chem Rev* 2018, **118**(16)**:** 7409-7531.

11. Stewart MP, Sharei A, Ding XY, Sahay G, Langer R, Jensen KF. In vitro and ex vivo strategies for intracellular delivery. *Nature* 2016, **538**(7624)**:** 183-192.

12. Chakravarty P, Qian W, El-Sayed MA, Prausnitz MR. Delivery of molecules into cells using carbon nanoparticles activated by femtosecond laser pulses. *Nat Nanotechnol* 2010, **5**(8)**:** 607-611.

13. Baumgart J, Humbert L, Boulais E, Lachaine R, Lebrun JJ, Meunier M. Off-resonance plasmonic enhanced femtosecond laser optoporation and transfection of cancer cells. *Biomaterials* 2012, **33**(7)**:** 2345-2350.

14. Lukianova-Hleb EY, Ren XY, Zasadzinski JA, Wu XW, Lapotko DO. Plasmonic Nanobubbles Enhance Efficacy and Selectivity of Chemotherapy Against Drug-Resistant Cancer Cells. *Adv Mater* 2012, **24**(28)**:** 3831-3837.

15. Heinemann D, Kalies S, Schomaker M, Ertmer W, Escobar HM, Meyer H*, et al.* Delivery of proteins to mammalian cells via gold nanoparticle mediated laser transfection. *Nanotechnology* 2014, **25**(24).

16. Lakshmanan S, Gupta GK, Avci P, Chandran R, Sadasivam M, Jorge AES*, et al.* Physical energy for drug delivery; poration, concentration and activation. *Adv Drug Deliver Rev* 2014, **71:** 98-114.

17. Sengupta A, Kelly SC, Dwivedi N, Thadhani N, Prausnitz MR. Efficient Intracellular Delivery of Molecules with High Cell Viability Using Nanosecond-Pulsed Laser-Activated Carbon Nanoparticles. *Acs Nano* 2014, **8**(3)**:** 2889-2899.

18. Xiong RH, Samal SK, Demeester J, Skirtach AG, De Smedt SC, Braeckmans K. Laser-assisted photoporation: fundamentals, technological advances and applications. *Adv Phys-X* 2016, **1**(4)**:** 596-620.

19. Liu J, Xiong RH, Brans T, Lippens S, Parthoens E, Zanacchi FC*, et al.* Repeated photoporation with graphene quantum dots enables homogeneous labeling of live cells with extrinsic markers for fluorescence microscopy. *Light-Sci Appl* 2018, **7**.

20. Soenen SJ, Rivera-Gil P, Montenegro JM, Parak WJ, De Smedt SC, Braeckmans K. Cellular toxicity of inorganic nanoparticles: Common aspects and guidelines for improved nanotoxicity evaluation. *Nano Today* 2011, **6**(5)**:** 446-465.

21. Soenen SJ, De Cuyper M, De Smedt SC, Braeckmans K. Chapter ten - Investigating the Toxic Effects of Iron Oxide Nanoparticles. In: Düzgüneş N (ed). *Methods in Enzymology*, vol. 509. Academic Press, 2012, pp 195-224.

22. Soenen SJ, Manshian B, Montenegro JM, Amin F, Meermann B, Thiron T*, et al.* Cytotoxic Effects of Gold Nanoparticles: A Multiparametric Study. *Acs Nano* 2012, **6**(7)**:** 5767-5783.

23. Joris F, Manshian BB, Peynshaert K, De Smedt SC, Braeckmans K, Soenen SJ. Assessing nanoparticle toxicity in cell-based assays: influence of cell culture parameters and optimized models for bridging the in vitro-in vivo gap. *Chem Soc Rev* 2013, **42**(21)**:** 8339-8359.

24. Soenen SJ, Manshian BB, Abdelmonem AM, Montenegro JM, Tan S, Balcaen L*, et al.* The Cellular Interactions of PEGylated Gold Nanoparticles: Effect of PEGylation on Cellular Uptake and Cytotoxicity. *Part Part Syst Char* 2014, **31**(7)**:** 794-800.

25. Malysheva A, Ivask A, Doolette CL, Voelcker NH, Lombi E. Cellular binding, uptake and biotransformation of silver nanoparticles in human T lymphocytes. *Nat Nanotechnol* 2021.

26. Harizaj A, Descamps B, Mangodt C, Stremersch S, Stoppa A, Balcaen L*, et al.* Cytosolic delivery of gadolinium via photoporation enables improved in vivo magnetic resonance imaging of cancer cells. *Biomaterials Science* 2021.

27. Huang C, Soenen SJ, Rejman J, Lucas B, Braeckmans K, Demeester J*, et al.* Stimuli-responsive electrospun fibers and their applications. *Chem Soc Rev* 2011, **40**(5)**:** 2417-2434.

28. Lv D, Zhu MM, Jiang ZC, Jiang SH, Zhang QL, Xiong RH*, et al.* Green Electrospun Nanofibers and Their Application in Air Filtration. *Macromol Mater Eng* 2018, **303**(12).

29. Yamanaka S. Pluripotent Stem Cell-Based Cell Therapy—Promise and Challenges. *Cell Stem Cell* 2020, **27**(4)**:** 523-531.

30. Bargehr J, Ong LP, Colzani M, Davaapil H, Hofsteen P, Bhandari S*, et al.* Epicardial cells derived from human embryonic stem cells augment cardiomyocyte-driven heart regeneration. *Nature biotechnology* 2019, **37**(8)**:** 895-906.

31. Pavel-Dinu M, Wiebking V, Dejene BT, Srifa W, Mantri S, Nicolas CE*, et al.* Gene correction for SCID-X1 in long-term hematopoietic stem cells. *Nature Communications* 2019, **10**(1)**:** 1634.

32. Fee T, Surianarayanan S, Downs C, Zhou Y, Berry J. Nanofiber Alignment Regulates NIH3T3 Cell Orientation and Cytoskeletal Gene Expression on Electrospun PCL+Gelatin Nanofibers. *Plos One* 2016, **11**(5)**:** e0154806.

33. Schmader KE, Hanlon JT, Pieper CF, Sloane R, Ruby CM, Twersky J*, et al.* Effects of geriatric evaluation and management on adverse drug reactions and suboptimal prescribing in the frail elderly. *The American journal of medicine* 2004, **116**(6)**:** 394-401.

34. DiTommaso T, Cole JM, Cassereau L, Buggé JA, Hanson JLS, Bridgen DT*, et al.* Cell engineering with microfluidic squeezing preserves functionality of primary immune cells in vivo. *Proc Natl Acad Sci U S A* 2018, **115**(46)**:** E10907-e10914.

35. Zhang M, Ma Z, Selliah N, Weiss G, Genin A, Finkel TH*, et al.* The impact of Nucleofection® on the activation state of primary human CD4 T cells. *Journal of immunological methods* 2014, **408:** 123-131.

Methods

Fabrication of photothermal nanofibers.

Polycaprolactone (PCL, Molecular Weight= ~70,000 g/mol), N, N-Dimethylformamide (DMF), Tetrahydrofuran (THF) and iron oxide (Fe_3O_4) nanopowder (#MKBW3262, Sigma-Aldrich, Belgium) were purchased from Sigma-Aldrich (Belgium). The iron oxide nanopowder was re-dispersed in 2 mL of a 1:1 DMF/THF solution to which 480 mg of dried PCL was added. This mixture was used for electrospinning of fibers which were collected on microscope glass slides (#1000912, Marienfeld, Germany) mounted on the grounded rotating collector as shown in **Supplementary Fig. 1**. During electrospinning, unless otherwise specified, the applied voltage, flow rate and electrospinning distance were fixed at 10 kV, 0.3 mL/h and 20 cm, respectively. The grounded rotating collector was set at a rotating speed of 500 rpm. After 30 min (or specifically indicated time) the electrospinning process was stopped and glass slides with the nanofiber web were separated from the rotating collector and sterilized by UV irradiation for 45 min in a laminar flow cabinet (**Supplementary Fig. 2**).

Fabrication of home-made PEN cell culture substrates.

8-well Secure-Seal™ double sided adhesive spacers (#S24737, Invitrogen) were sterilized by UV irradiation for 45 min in a laminar flow cabinet (**Supplementary Fig. 2b**). After removing the protective sealing from one side of the adhesive spacers, they were gently stuck on the nanofiber web (**Supplementary Fig. 2c**). Next, these samples were immersed in DI water for 3 min for easy removal of the web (with adhesive spacers on top) from the glass slides. The web was manually cut into smaller pieces with either one or 4 adhesive wells per piece (into which cells can be grown) and stored in PBS buffer.

Next, these PEN cell culture substrates were further modified with collagen for optimal cell attachment as schematically shown in **Supplementary Fig. 3a**. Poly(allylamine hydrochloride) (PAH, Mw=17,560 g/mol, #MKBZ2824V, Sigma-Aldrich, Bornem, Belgium) and concentrated sulfuric acid solution (96%) were purchased from Sigma-Aldrich. Collagen I Rat Protein was purchased from Thermo Fisher Scientific (#A1048301, Gibco™, Belgium). 4-well PEN cell culture substrates were immersed in 32% sulfuric acid solution (3 mL per well of 6-well plate) for 3 min. After washing with distilled water, they were immersed into an aqueous solution of the polyelectrolyte PAH (2 mg/mL, 0.5 M NaCl) for 15 min and rinsed 3 times with distilled water. Physisorption of PAH to the nanofiber surface made the fibers positively charged. Next, the PAH coated fibers were immersed in a 0.5 mg/mL aqueous solution of Collagen I Rat Tail Protein for 15 min and rinsed with PBS solution. Hydrated fibers were formed through surface

hydrolysis, for which PCL-fibers were soaked for more than 1 hour in 0.1 M NaOH at 4°C and rinsed with PBS solution. Finally, the modified PEN substrates were stored in PBS before further use.

Culturing or collecting HeLa and Jurkat cells in the PEN cell substrates for photoporation treatment.

HeLa cells (#CCL-2) and Jurkat clone E6.1 (#TIB-152) were obtained from ATCC and employed as model for the transfection of respectively adherent and suspension cells by PEN photoporation. Human lung epithelial cells (H1299) stably expressing enhanced green fluorescent protein (GFP) were used for the validation of siRNA knockdown experiments. HeLa cell culture medium was made from DMEM/F-12 with 2 mM glutamine, 100 U/mL penicillin/streptomycine and 10% heat–inactivated fetal bovine serum (FBS). H1299 and Jurkat cell culture medium consisted of RPMI1640 with 2 mM glutamine, 100 U/mL penicillin/streptomycine and 10% FBS.

To grow adherent cells, PEN cell culture substrates were placed in 6-well titer plates (#10062-892, VWR) to which HeLa or H1299 were added (~1×10^6 cells in 2 mL cell culture medium). Cells were allowed to attach and grow during 24 h in a cell incubator at 37 °C in a humidified atmosphere with 5% CO_2. Just prior to photoporation treatment, the molecules of interest that need to be delivered into the cells were added to the cell medium.

Jurkat cells were cultured in 75 cm^2 or 182.5 cm^2 flasks (#734-2313, #734-2315, VWR) at a cell density between 1×10^5 and 1×10^6 cells/mL. For photoporation, the molecules of interest were added to the cell medium and cells were transferred to the PEN cell substrates at ~2×10^5 cells/well. Cells were allowed to sediment on the fiber web during 5 min before starting the photoporation laser scanning.

Laser irradiation of cells on PEN substrates.

Photoporation requires cells to be irradiated with laser light. Here we used a custom-built optical set-up as previously reported with some minor modifications[36, 37]. Briefly, a pulsed laser with 7 ns pulse duration was tuned at wavelength of 647 nm (Opolette™ HE 355 LD, OPOTEK Inc, CA) and applied to irradiate the PEN substrates. The collimated pulsed laser beam was directed through a 1° Light Shaping Diffuser (Physical Optics Corporation, Torrance, CA), which in combination with an achromat lens in front of the microscope entrance and a 20X objective lens (Plan Fluor, Nikon) resulted in a laser beam diameter of ~250 µm at the sample. The laser pulse energy was monitored by an energy meter (J-25MB-HE&LE, Coherent) synchronized to the pulsed laser. In order to scan all the cells on the PEN substrates (diameter

of ~9 mm), a motorized microscope stage was used to scan the sample through the stationary laser beam line by line. As the laser repetition rate was 20 Hz, the scanning speed was set at 3 mm/s with a distance between subsequent line of 0.15 mm. In this way, all cells received at least one laser pulse up to maximally 4 in the overlapping regions between neighboring irradiation zones. In some experiments with Jurkat or human T-cells, the cells were scanned multiple times, as indicated in the main text. In that case the cells were re-suspended within the PEN well and allowed to sediment again between each scan in order to let the cells randomly attach to the nanofibers at new locations.

IONP-sensitized traditional photoporation of cells.

Polyethyleneimine (PEI) functionalized iron oxide nanoparticles (IONPs) were prepared by dispersing 100 mg of iron oxide powder (Iron Oxide Fe_3O_4 Nanopowder, #MKBW3262, Sigma-Aldrich, Belgium) in a 10 mL solution of 10 wt% branched PEI (bPEI, 25 kDa, Sigma-Aldrich) immediately followed by sonicated for 1 minute with a tip sonicator (10% A, Branson Digital Sonifier, Danbury, USA). The mixture was then further sonicated with a bath sonicator (Branson 2510 Branson Ultrasonics, Dansbury, CT, USA) for an additional 1 hour and then vigorously stirred overnight to allow PEI molecules to absorb on the surface of IONPs. Next, the unbound bPEI was removed by performing several washing steps with HyClone water (VWR) via centrifugation (4000 X g, 10 minutes). Finally, PEI-coated IONPs with an appropriate size were selected via differential centrifugation. The physicochemical characterization (i.e., hydrodynamic diameter, zeta-potential and particle concentration) was performed respectively with dynamic light scattering (DLS, Zetasizer Nano-ZS, Malvern instruments Co., Ltd) (= hydrodynamic diameter and zeta-potential) and/or with Nanoparticle Tracking Analysis (NTA, NanoSight LM10, Malvern Panalytical, UK) (= hydrodynamic diameter and particle concentration).

For IONP-sensitized photoporation, HeLa cells were grown in a 96-well plate (#10062-900, VWR®, US) at a density of 1×10^4 cells per well. Next, cells were incubated for 30 min at 37°C with PEI coated IONPs at various concentrations as indicated. Cells were subsequently photoporated at the indicated laser fluence in the presence of 2 mg/mL FD10 dissolved in cell culture medium.

Detection of vapour nanobubbles.

The generation of vapour nanobubbles was detected by dark-field microscopy as they efficiently scatter light. As VNBs typically have a very short lifetime (< 1 µs), depending on their size, we synchronized the camera (EMCCD camera, Cascade II: 512, Photometrics, Tucson,

USA) with the pulsed laser by an electronic pulse generator (BNC575, Berkeley Nucleonics Corporation, CA, USA). The pulse laser sends a Q-switch signal to trigger pulse generator and it will trigger the camera at a setting delay.

Detection of reactive oxygen species (ROS).

ROS formation was evaluated with the probe 2', 7'-Dichlorofluorescin (DCFH) as a fluorescence indicator, as reported before[38, 39]. Briefly, DCFH was prepared by mixing 0.5 mL of 1 mM DCFH-DA (2', 7'-Dichlorofluorescin diacetate, purchased from Sigma (# D6883) in methanol with 2.0 mL of 0.01 N NaOH for 30 min at room temperature. The mixture was neutralized with 10 mL of 25 mM NaH_2PO_4 to PH 7.2. All reactions were performed in 40 mM Tris-HCl in a total volume of 1 mL containing 25 µl DCFH solution and 10 µM Fe^{2+} (from $FeSO_4$).

To measure the amount of ROS generation by laser irradiation of the PEN substrates, 150 µl DI water was added to the PEN wells before starting the laser scanning procedure. After treatment, the DI water was collected again from the PEN wells and added to the DCFH solution. A negative control was included which did not receive laser treatment, while a positive control sample was prepared from 150 µl H_2O_2 added to the DCFH solution.

After further incubation for 2 h at 37 °C, fluorescence was measured by a Victor3 microplate reader (#1420-040, PerkinElmer, Turku, Finland) with excitation at 485 nm and emission at 535 nm. Relative fluorescence intensity (FI) was calculated by equation (1):

$$Relative\ FI = \frac{FI_S - FI_{BG}}{FI_{CTRL} - FI_{BG}} \quad (1)$$

Where FI_S is the fluorescence intensity of the actual sample, FI_{BG} is the fluorescence intensity of the background which is just water as blank sample, and FI_{CTRL} is the fluorescence intensity of the DCFH solution.

Electron and confocal microscopy.

For TEM imaging, the nanofibers were directly electrospun on carbon-coated Cu grids (200-mesh). Following laser irradiation of the nanofibers, they were visualized by a JEM 1400 plus transmission electron microscope (JEOL, Tokyo, Japan) operated at 20-60 kV. For SEM imaging, samples were first coated with 5nm platinum using a Quorum Q150T ES sputter coater. Scanning electron microscope images were taken with a Zeiss Crossbeam 540 Electron Microscope using a SE2 detector at 20 kV.

For visualization by confocal microscopy, fluorescent PCL nanofibers were fabricated by electrospinning a PCL solution mixed with the fluorophores 3-(2-benzothiazolyl)-7-

(diethylamino) coumarin (coumarin-6, #12779, Sigma-Aldrich). A confocal laser scanning microscope (C1si, Nikon, Japan) with 60X water lens (Plan Apo VC, Nikon) was used to image the fluorescent PCL nanofibers. HeLa and H1299 cells grown on PEN substrates were imaged by the C1si confocal with a 10X lens (CFI Plan Apochromat, Nikon). For confocal imaging of Jurkat cells, their plasma membrane was stained with 10 µg/mL deep red fluorescent CellMask (#C10046, ThermoFisher Scientific). A series of z-stack confocal images were acquired in two channels (green channel recorded for nanofibers and deep red channel for the cells) with the 60X water lens.

Quantification of intracellular delivery by flow cytometry.

Photoporation efficiency was quantified by flow cytometry. For HeLa's we used 10, 40, 70, 150, and 500 kDa FITC-dextran or 10 kDa Alexa Fluor® 647 labelled dextran as model compounds, which were added to the cells at a final concentration of 2 mg/mL or of 0.5 mg/mL, respectively. Before 24 h laser treatment, 1 million HeLa cells in 2 mL cell culture medium were added to the 6-well plate containing 4 PEN subtract well dishes.

After photoporation on the PEN substrates, HeLa or H1299 cells were detached by 0.25% trypsin-EDTA (Invitrogen, Belgium) treatment and collected by 5 min 300 X g centrifugation. To collect Jurkat or Human CD3+ T cells, the PEN substrates were simply washed one or two times with PBS. Next, collected cells were re-suspended in flow buffer (PBS supplemented with 5% FBS) and measured by flow cytometry (CytoFLEX Cytometer, Beckman Coulter, Belgium) until at least 10000 events were detected per sample. The cells loaded with FITC-dextran or Alexa Fluor® 488 labelled siRNA were excited with a 488 nm laser and fluorescence was recorded in the 525/40 channel. On the other hand, when the cells were loaded with Alexa Fluor® 647 labelled dextran or labelled with PD1APC antibody (see below), a 638 nm laser was used to excite the cells and the fluorescence was detected in the 660/10 channel.

The following antibodies were used for flow cytometry analysis of human CD3+ T cells: CD3 BV421 (Pacific blue), CD4 BB700 (PERCP-Cy5.5), CD8 APC-Cy7 and PD1APC (Invitrogen, Belgium). Briefly, T cells were washed with PBS (PBS, Gibco-invitrogen) and re-suspended in FACS buffer, supplemented with 5% bovine serum albumin, BSA (Sigma-Aldrich, Bornem, Belgium). After a 30 min incubation at 4°C with the indicated antibodies, the cells were washed and analyzed by flow cytometry. Pacific blue and PERCP-Cy5.5 were excited with a 405 nm and 488 nm laser with filter of 450/50 and 690/50, respectively. APC-Cy7 and APC was excited 638 nm laser with filter of 660/20 and 780/60, respectively. Control samples are used

to define the threshold for positive cell loading, where the threshold value is defined as the 95% level of controlled cells.

Evaluation of cell viability.

In this work, two methods were employed to evaluate cell viability. To visualize dead cells with confocal microscopy, or to exclude them from flow cytometry analysis, Calcein AM (#C3100MP, Invitrogen™) was used as a viability stain. Viable cells will be positive for calcein fluorescence, while dead cells will not. Before analysis, cells were incubated for 30 min at room temperature with Calcein AM. For more accurate quantification of cell viability, the CellTiter-Glo® Luminescent cell viability assay (#G7571, Promega, Belgium) was used, which is based on the quantitation of ATP. After photoporation treatment, cell culture medium was removed and 100 µL CellTiter-Glo reagent solution was added to each sample together with 100 µL fresh cell medium. The samples were put on a shaker at 100 rpm for 10 min at room temperature. Finally, 100 µL solution was again removed from each sample and transferred to 96 titer well plates (#655075, Greiner Bio-one, Germany) for analysis by a microplate reader (GloMax ®, Progmega, Belgium).

Quantification of cell loading and viability by imaging process.

The imaging processing quantification method was reported in our previous work[1]. Briefly, after laser treatment, 3-5 confocal images were acquired with a confocal laser scanning microscope (C1si, Nikon, Japan) using a 10× lens (CFI Plan Apochromat, Nikon, Badhoevedorp, The Netherlands). Each image consists of green fluorescence (viability) and red fluorescence (loading efficiency) channels. A Matlab (The matworks, Natick, MA, USA) program was written for automated quantification of cell loading and cell viability. Untreated cells are used to define the threshold for positive cell loading, where the threshold value is defined as the 95% level of untreated cells. Similarly, cells are considered as alive when the green fluorescence intensity is higher than the 95% level of dead cells.

Quantitative Fe assay via ICP-MS/MS.

The determination of Fe by means of inductively coupled plasma – mass spectrometry (ICP-MS) is hampered by the occurrence of spectral interference. Therefore, tandem ICP-mass spectrometry (ICP-MS/MS) was used instead and interference-free conditions were obtained by relying on chemical resolution using a reactive gas mixture of NH_3/He (1:9). Method optimization revealed that a mass-shift approach, whereby Fe was monitored under the form of the reaction product ion $Fe(NH_3)_2^+$ provided the best conditions[40]. This method was used to evaluate the potential release of IONPs from the fibers in the presence or absence of cells. In

the absence of cells, DI water was added to the PEN substrates and was collected after laser treatment. Samples with cells were prepared as described earlier. After laser irradiation, the cells were collected by washing with PBS or by trypsinizing in the case of suspension and adherent cells, respectively. Finally, 100 µL *aqua regia* (3:1 HCl/HNO_3) was added to the samples to digest the cells and other potentially present organic matter. The sample solutions were diluted 100 times with 2% HNO_3 to a final volume of 10 mL in metal-free tubes, adding Y as internal standard at a final concentration of 1 µg/L (1,000 mg/L Y standard stock solution, Inorganic Ventures, Christiansburg, VA, USA) to correct for instrument instability and/or signal drift. External calibration standards (0, 0.5, 1, 2.5, 5 and 10 µg/L Fe + 1 µg/L Y) were prepared by appropriate dilution of a 1000 mg/L Fe standard stock solution (Inorganic Ventures, Christiansburg, VA, USA) in 2% HNO_3, mimicking the matrix of the sample solutions. During all steps of the sample preparation, the solutions were mixed thoroughly using a vortex mixer. The tandem ICP-MS instrument (Agilent 8800 triple-quadrupole ICP-MS, Agilent Technologies, Japan) was tuned on a daily basis for high sensitivity across the mass range and low oxide ion formation to achieve optimal conditions for the interference-free determination of Fe. The determination of Fe was based on external calibration with internal standardization for which the $^{56}Fe(NH_3)_2^+$ signal intensity was normalized using the $^{89}Y(NH_3)_6^+$ signal intensity. A methodological detection limit of 80 µg/L was determined by multiplying the instrumental background-equivalent concentration (BEC) by the dilution factor (100x).

Simulations of PEN photothermal response.

Numerical simulations were performed to get a deeper understanding of the photothermal response of PEN fibers to nanosecond pulsed laser irradiation. First, the laser-induced heating of IONPs was computed using the Generalized Multiparticle Mie Theory (GMM) as described elsewhere[41, 42]. It provides a rigorous description of the interaction of electromagnetic waves with (aggregates of) spherical particles, whose composition is determined by the real and imaginary part of their dielectric constant. In the GMM method, scattered fields from each individual sphere are solved in terms of the respective sphere-centered reference systems. In order to solve multisphere-scattering through the Mie-type multipole superposition approach, the incident plane wave is expanded in terms of vector spherical wave functions in each of the sphere-centered coordinate systems, obtaining the total electromagnetic field incident upon each sphere in the particle cluster, which consist of two parts: (1) the initial incident plane wave and (2) the scattered waves from all other spheres in the aggregate. In a next step, a single field representation for the total scattering field from the aggregate as a whole by expanding it in vector spherical wave functions is generated. Finally, with the total scattered

field available, and based on the analytical expressions for the amplitude scattering matrix of an aggregate of spheres, it is possible to derive a rigorous formula for other fundamental scattering properties such as extinction, absorption, and scattering cross sections. In all calculations presented in this work the dielectric function tabulated by Querry for iron oxide (magnetite) was employed[43]. The calculations were performed for 160 nm particles in water (n = 1.33) or PCL (n = 1.46). As the GMM code is restricted to applications in homogeneous media, for calculations at the polymer-water interface we have used the effective medium approximation[44]. Here, we considered that particles were immersed in a dielectric environment with an effective refractive index of n_{eff} = 1.40, considering that half of the IONPs are exposed to the aqueous medium. The calculations for linear arrangements of IONPs were performed with an inter-particle distance of 1 nm.

Heat transfer from IONPs to the nanofiber PCL matrix and to the surrounding medium was simulated by a commercial CFD (Computation Fluid Dynamics) software package (ANSYS FLUENT) which allows to numerically solve the heat transfer equation. The simulation procedure was as follows. As shown in **Supplementary Fig. 10c**, a 3D geometry model was built with a simulation domain of 6 µm × 6 µm × 36 µm including a cylindric domain (diameter=0.32 µm, length=30 µm) to represent a nanofiber and a spherical domain (diameter=0.16 µm) representing a single IONP. The simulation domain is discretized into a grid with a total of 2.85 million elements (the smallest mesh size was 30 nm, **Supplementary Fig. 10d**). The boundary conditions were set as infinite boundary conditions. The initial temperature of IONPs were set according to the Mie theory calculations discussed above. The IONPs temperature were maintained for 7 ns this was the duration of the laser pulses used in this work. PCL polymer specific heat and thermal conductivity were set at 1250 J/kg-K and 0.175 W/m-K respectively[45]. For the water surrounding the fiber a specific heat of 4182 J/kg-K and a thermal conductivity of 0.6 W/m-K were used.

Calculation of the temperature increasing of bulk water.

The total absorption energy by IONPs embedded in fibers was simply calculated as:

$$Q_{IONPs} = C_{IONPs} \times m_{IONPs} \times \Delta T_{IONP} \quad (3)$$

Here, *C* is the heat capacity of IONPs, *m* is the mass of IONPs in a one PEN web dish and *ΔT* is the single IONP temperature increase after laser irradiation which is calculated by IONPs absorption cross section multiplying with laser fluence. Here, we assume that all IONPs heat

energy finally transfer to the surrounding water causing the bulk temperature increasing as calculating as following: $\Delta T_{water} = \frac{Q_{IONPs}}{C_{water} \times m_{water}}$.

siRNA transfections for downregulation of GFP in H1299.

For siRNA transfections of H1299 cells, twenty-one nucleotide siRNA duplexes targeting the enhanced green fluorescent protein (siGFP) and negative control duplexes (siCTRL) were ordered from Eurogentec (Seraing, Belgium). siGFP: sense strand = 5'-CAAGCUGACCCUGAAGUUCtt-3'; antisense strand= 5'-GAACUUCAGGGUCAGCUUGtt-3'. siCTRL: sense strand = 5'-UGCGCUACGAUCGACGAUGtt-3'; antisense strand = 5'-CAUCGUCGAUCGUAGCGCAtt-3'. To quantify intracellular delivery after PEN photoporation, siCTRL duplex was labeled with Alexa Fluor® 488 (Eurogentec). Before 24 h laser treatment, 1 million H1299 cells in 2 mL cell culture medium were added to the 6-well plate containing 4 PEN subtract well dishes. The amount of siRNA was added to the cells in final concentration of 1 µM except specifically indicating.

For calculating siRNA gene silencing efficiency, GFP knockdown efficiency was calculated according to equation (4):

$$\text{Knockdown efficiency } (\%) = \left(1 - \frac{FI_{GFP}+}{FI_{NTC\_GFP}+}\right) \times 100\% \quad (4)$$

Here, $FI_{GFP}+$ is the percentage positive cells in fluorescence intensity treated with anti-GFP siRNA and $FI_{NTC\_GFP}+$ is the percentage positive cells in fluorescence intensity in nontreated control samples. The data obtained from flow cytometery was post-processed with the FlowJo software package (Treestar Inc, Ashland, USA).

Intracellular delivery of RNPs Cas9 for knockout of GFP in H1299 cells.

crRNA: tracrRNA duplexes were prepared by mixing individual crRNAs in a 1:1 molar ratio with tracrRNA, followed by heating at 95°C for 5 minutes and annealing at room temperature for 5-10 minutes. Next, Cas9 RNP complexes were obtained by mixing either crRNA:tracrRNA duplexes in a 2.5:1 molar ratio with Cas9 endonuclease and allowing the complexes to assemble for at least 10 minutes at room temperature prior delivery. H1299 cells were seeded on the PEN cell culture substrates as described above prior to PEN photoporation. On the day of photoporation, Cas9 RNPs were prepared as described above. RNP complexes were diluted in Opti-MEM at a final concentration as indicated in the main text, and added to the cells followed by photoporation by laser scanning. Post laser treatment, the cells were washed once with DPBS-, supplied with new culture medium and further incubated at 37°C, 5% CO2

prior to analysis of GFP knockout by confocal microscopy or flow cytometry. RNP gene knockout efficiency was calculated by equation (5):

$$\text{Knockout efficiency } (\%) = \left(1 - \frac{FI_{RNP\_GFP}}{FI_{NTC}}\right) \times 100\% \quad (5)$$

Here, FI_{RNP_GFP} is the mean fluorescence intensity of cells treated with RNPs for knockout of eGPF and FI_{NTC} is the mean fluorescence intensity of non-treated cells.

PEN photoporation and electroporation of human embryonic stem cells.

The H9 human embryonic stem cell (hESC) line (WA09, WiCell, feeder free cultures were obtained via prof. C. Verfaillie, KULeuven, Belgium) was employed for all PEN and EP experiments. Culturing was done feeder-free on Geltrex coatings (# A1413302, Invitrogen) in Essential 8 medium (#A1517001, Invitrogen) supplemented with 1:100 Penicillin/Streptomycin (# 15140-122, Invitrogen). Passaging of hESCs was done with TrypLE Select (# 12563011, Invitrogen).

Prior to cell seeding, PEN cell culture substrates were coated overnight with 1:100 Geltrex on an orbital shaker platform. Next, $5x10^4$ hESCs were seeded on the PEN cell culture substrates. After 1h of incubation at 37°C in a humidified atmosphere with 5% CO_2 and 5% O_2, 1 mL of E8 Essential medium supplemented with 1:100 RevitaCell (A2644501, Invitrogen) was added to the 12 wells. After 24h, the medium was replaced by Essential 8 medium and refreshed daily till the cell density achieved the required density in 3-4 days.

Before PEN photoporation, 0.5 mg/ml 10 kDa Alexa Fluor® 647 labelled dextran in cell medium was added to the cells. Post laser scanning at the indicated laser fluence, cells were further cultured for another 2 h before recording confocal microscopy images. Cell viability was determined by Cell Titer-Glo at the indicated times post treatment. Cell proliferation was quantified from confocal microscopy images as well as described below.

Electroporation using the P3 Primary Cell 4D-Nucleofector™ X Kit (Lonza, Cologne, Germany) with a Nucleofector™ 4D (Lonza, Cologne, Germany) was used to deliver 10 kDa Alexa Fluor® 647 labelled dextran, according the manufacture's protocols. In brief, 2×10^5 single hESCs were re-suspended in the Nucleofector™ solution supplemented with a final concentration of 0.5 mg/mL Alexa Fluor® 647 labelled dextran. This solution containing cells was transferred to a 20 µL Nucleofector™ strip and electroporated using the indicated programs. For electroporation hESCs were detached with TrypLE, transferred to an electroporation cuvette and treated with the selected program[46, 47]. After electroporation, the cells were washed with cell culture medium and transferred to a 48-well plate for further incubation at 37°C. Finally,

delivery efficiency was quantified from confocal microscopy images and cell viability was measured by Cell Titer-Glo at the indicated times post treatment.

Directed differentiation towards cardiomyocytes was done with the PSC Cardiomyocyte Differentiation Kit (# A2921201, Invitrogen) according to manufacturer's protocol. hESC and cardiomyocytes staining protocols were performed as follows. hESCs and cardiomyocytes were fixed for 20 min with 4% paraformaldehyde at RT. hESCs were permeabilized for 30 min with 0.1% Triton X-100 diluted in phosphate buffered saline (PBS). Subsequent incubation with blocking solution consisting of 5% Goat serum (#16210-064, Invitrogen) in PBS was done for 30 min. The cells were incubated overnight at 4 °C with primary antibodies diluted in PBS containing 0.05% Tween20 and 1% bovine serum albumin (BSA). The used antibodies are listed in **Supplementary Table 3**. The next day, cells were incubated for 30 min at RT with secondary antibodies diluted in PBS containing 0.05% Tween20 and 1% BSA and subsequently incubated for 10 min with 0.1% Hoechst solution (#H3570, Invitrogen). Immunostaining of CMs was performed as previously described[48] with the exception that the primary antibody was incubated overnight at 4°C.

Single guide RNA targeting the IL-2R gamma gene (sequence: 5'-GGTAATGATGGCTTCAACA-3') was purchased from Synthego. Cas9 RNP complexes were simply made by mixing either sgRNA in a 2.5:1 molar ratio with Cas9 endonuclease and allowing the complexes to assemble for at least 10 minutes at room temperature prior delivery. Extraction of genomic DNA was done using the innuPREP DNA Mini Kit (Analytik Jena, Jena, Germany) according the manufacturer's protocol. Genomic DNA of H9 stem cells was extracted using the InnuPREP DNA mini kit (Analytik Jena, Jena, Germany), according manufacturer's instructions. Next, a target DNA region in the IL-2R gamma gene was amplified using 100 ng genomic template DNA and the KAPA HiFi HotStart ReadyMix (Roche Diagnostics Belgium, Diegem, Belgium), and with forward primer 5'-ACCACCTTACAGCAGCACC-3' and reverse primer 5'-ATGATGGTCAGAAGGAGGAGG-3'. PCR cycling conditions consisted of initial denaturation of 2 minutes at 98°C, followed by 35 cycles of denaturation at 98°C (10 seconds), annealing at 65°C (30 seconds), elongation at 72°C (21 seconds), and a final elongation at 72°C for 10 minutes. Amplified PCR products were purified using the by the QIAquick PCR purification kit (Qiagen, Chatsworth, CA, USA), according the manufacturer's protocol. The sequence of the PCR amplicons was eventually determined using Sanger sequencing by the GATC Lightrun service (Eurofins Genomics, Ebersberg, Germany) and using sequencing primer 5'-AGGACTTAGCCCGTGTC-3'. Knock-out levels were determined by Inference of CRISPR Edits

(ICE) analysis (Synthego), using a nontreated sample as unedited control and assuring a model fit of $R^2 > 0.9$.

PEN photoporation and electroporation of human CD3+ T cells.

Human T cells were obtained from Ghent University hospital. Buffy coats were obtained from healthy donors after informed consent and approval. Peripheral blood mononuclear cells (PBMCs) were isolated via density centrifugation using Lymphoprep (Alere Technologies, Oslo, Norway). Next, PBMCs were incubated in IMDM (Gibco, Invitrogen, Merelbeke, Belgium) supplemented with 10% fetal calf serum ((FCS, Bovogen), 100 U/mL penicillin (Gibco, Invitrogen), 100 µg/mL streptomycin (Gibco, Invitrogen), 2 mM glutamine and 5 ng/mL IL-2 (Roche, Vilvoorde, Belgium) and stimulated with CD23/CD28 activator (Stemcell Technologies, Vancouver, Canada r) at a 1:1 bead to cell ratio. After 7 days the cells were harvested and re-incubated with X-ray irradiated (40 Gy) (SARRP) PBMCs (1:2 ratio) and X-ray irradiated (50 Gy) JY (5:1 ratio) feeder cells in complete IMDM supplemented with 1 µg/mL phytohemagglutinin (Remel Europe, KENT, UK). After an additional 14 days, CD3+ cells were harvested and used for experiments as further indicated. Feeder cells were irradiated using the Small Animal Radiation Research Platform (Xstrahl, Surrey, UK). For photoporation treatment, T-cells were transferred to the culture substrates at a density of ~8×10^5 cells/well and already in the presence of the transfection molecules (if any). Cells were allowed to sediment on the fiber web for 5 min before starting the laser treatment.

CD70-specific CAR T cells were manufactured as previously described[49]. Briefly, PBMCs were isolated via Lymphoprep and T cells were stimulated using Imunocult Human CD3/CD28/CD2 activator in complete IMDM supplemented with 10 ng/mL IL-12 (PeproTech, Hamburg, Germany). Cells were harvested 72 hours after stimulation and resuspended in retroviral supernatant. Next, cells were centrifuged for 90 min at 1000× g (32°C) on retronectin coated plates (TaKaRa, Saint-Germain-en-Laye, France). Irradiated PBMCs (40 Gy) and irradiated JY cells (50 Gy) were used as allogenic feeder cells to expand transduced cells in completed IMDM supplemented with 1 µg/mL phytohemagglutinin (PHA, Sigma–Aldrich). On day 5 and 10, 5 ng/ml IL-2 was added and every 7-14 days cells were restimulated.For photoporation treatment, CD3+ T-cells or CAR T-cells were transferred to the culture substrates at a density of ~1.0×10^6 cells/well and already in the presence of the transfection molecules. Cells were allowed to sediment on the fiber web for 5 min before starting the laser treatment.

FD10 kDa and siRNA were delivered in human T cells by electroporation using the P3 Primary Cell 4D-Nucleofector™ X kit (Lonza, Cologne, Germany) with a Nucleofector™ 4D (Lonza,

Cologne, Germany), according the manufacture's protocol. In brief, 1×10^6 CD3+ T cells or CAR T-cells were re-suspended in the Nucleofector™ solution supplemented with a final concentration of 2 mg/mL FD10 or 1 µM siRNA. The solution containing cells were transferred to 20 µL Nucleofector™ strip and electroporated using the program EO-100, EO-115 or FI-115. After electroporation, cells were washed with cell culture medium and transferred to a 96-well plate at 200 K cells per well for further incubation at 37°C. For siRNA transfection, viable human T cells were stimulated with Immunocult CD3/CD28 activator and 5 ng/ml IL-2 4 hours after treatment. After 24, 48 or 72 hours of incubation, cells were washed with PBS and analyzed using flow cytometry or confocal microscopy as indicated.

siRNA transfection and PD1 expression analysis of transfected T cells.

For siRNA transfections of human T cells, siRNA duplexes targeting programmed cell death protein 1 (PD-1) and negative control duplexes (siCTRL) were ordered from various manufacturers (**Supplementary Table 2**). Human T cells were PEN photoporated or electroporated as previously described, in the presence of the indicated concentration of siRNA. After treatment cells were washed twice with PBS and resuspended in complete IMDM at 2 x 10^5 cells per well in a 96-well plate (#10062-900, VWR®, US). After 4 hours, human T cells were stimulated with Immunocult Human CD3/CD28 activator (Stemcell Technologies, Vancouver, Canada) and 5 ng/ml IL-2 to upregulate PD1 expression unless otherwise specified (*e.g.* unstimulated condition). At the indicated timepoints PD1 expression was evaluated using flow cytometry. Briefly, human T cells were washed with PBS and re-suspended in FACS buffer. Next, T cells were incubated with PD1PE (Milteny Biotec, Germany) for 30 min at 4°C after which the cells were washed and incubated for 10 min with TO-PRO™-3-iodide. The data obtained from flow cytometery was post-processed with the FlowJo software package (Treestar Inc, Ashland, USA). TO-PRO™-3 iodide (APC channel) was used to exclude dead cells from further flow cytometry analysis. Knockdown efficiency of PD1 expression was calculated according to equation (6):

$$\text{Knockdown efficiency}\ (\%) = 100\% - \left(\frac{MFI_{sample} - MFI_{Unstimulated}}{MFI_{siCTRL} - MFI_{Unstimulated}}\right) \times 100\% \quad (6)$$

Here, MFI_{sample} is the mean fluorescence intensity of cells treated with PD1 siRNA; $MFI_{unstimulated}$ is the mean fluorescence intensity of unstimulated T cells under identical experimental conditions; MFI_{siCTRL} is mean fluorescence intensity of cells treated with negative control siRNA.

Characterization of T cell phenotype and intracellular Ca^{2+} analysis.

The following antibodies were used for flow cytometry analysis of human CD3+ T cells: CD3 BV421 (Pacific blue, Invitrogen, Belgium), CD4 BB700 (PERCP-Cy5.5, Invitrogen, Belgium), CD8 APC-Cy7 (Invitrogen, Belgium), CD137 PE (Biolegend, USA) ,CD154 FITC (Biolegend,USA), PD1APC (Invitrogen, Belgium) and PD1PE (Milteny Biotec, Germany). Briefly, T cells were washed with PBS (PBS, Gibco-invitrogen) and re-suspended in FACS buffer, supplemented with 5% bovine serum albumin (BSA, Sigma-Aldrich, Bornem, Belgium). After 30 min incubation at 4°C with the indicated antibodies, the cells were washed and analyzed by flow cytometry. Non-treated cells were used to set the 90% threshold value above which cells are considered positive %. Intracellular Ca^{2+} was measured using a Fluo-4 Direct™ Calcium Assay Kit (#F10471, Invitrogen) according to the manufacturer's instructions.

Analysis of T cell proliferation using confocal microscopy

After PEN photoporation or electroporation, using optimized delivery protocols (see main text), T cells were washed twice and seeded at 2 x 10^5 cells per well in a 96 well plate. After 4 hours T cells were stimulated with 5 ng/ml IL-2 and Immunocult human CD3/CD28 activator in complete IMDM. At the indicated timepoints T cells were washed and stained with Calcein AM and TO-PRO-3 iodide for 30 min in cell medium. Living cells were detected and quantified based on their green (Calcein AM positive, living cells) and red (TO-PRO-3 negative, dead cells) fluorescence levels using an A1R confocal microscope (Nikon, Badhoevedorp, The Netherlands) equipped with a perfect focus system and a X20 objective lens (CFI Plan Apochromat, Nikon, Badhoevedorp, The Netherlands). The software package ImageJ with the plugin of Analyze Particles was used for image processing.

Cytokine expression analysis of human T cells.

To analyze the cytokine secretion profile of electroporated or PEN-photoporated T cells, human T cells were seeded in a 96-well plate at 1 x 10^6 cells per well for up to 48 hours post-treatment. At the indicated time-points, supernatant was collected for cytokine secretion analysis. Cytokine secretion of 10 different cytokines, including IL-5, IL-6, IL-9, IL-10, IL-13, IL-17A, IFN-γ and TNF-α, was quantified using a multiplex bead assay (LEGENDplex, Biolegend) according to the manufacturer's instructions.

^{51} Chromium release cytotoxic killing assay.

Cytotoxic killing of CAR transduced T cells exposed to electroporation or PEN photoporation (without cargo molecules) was measured using a ^{51}Chromium release assay as previous described[50]. Both SKOV3 and H1650 cells were used as target cancer cell lines. CD70-specific

CAR T cells were PEN photoporated, electroporated or left untreated, as previously described, followed by 48 hours of culturing in complete IMDM supplemented with 5 ng/ml IL-2. Target cells were labeled with ^{51}Chromium (Perkin Elmer, Zaventem, Belgium) for 90 min at 37 °C. After several washing steps, 10^3 target cells were added per well in a 96 well V-bottom plates (NUNC, Thermo Fisher Scientific, Merelbeke, Belgium). Various amounts of CAR T cells were added at the indicated effector-target cell ratios. Next, supernatans was collected 4 hours later and measured in a 1450 LSC & Luminescence Counter (Perkin Elmer, Zaventem, Belgium). Specific lysis was calculated using the following formula: (experimental release–negative control release) / (positive control release–negative control release) × 100%. Here, negative control release is the release induced by only target cells in regular cell culture medium; positive control release is the release of the complete lysis of the target cells by adding 2% tritonis in cell culture medium; experimental release is the release of the samples under coordinate experimental conditions.

CAR-T treatment of SKOV3 mouse tumor model.

Buffy coats from healthy donors were obtained from the Belgian Red Cross and used following the guidelines of the Medical Ethical Committee of Ghent University Hospital, after informed consent had been obtained, in accordance with the Declaration of Helsinki. PBMCs were isolated by Lymphrop (StemCell Technologies) gradient centrifugation. The percentage of CD3+ cells was determined by flow cytometry and T cells were stimulated with Immunocult Human CD3/CD28/CD2 T cell activator (StemCell Technologies) according to the manufacturer's instructions. Cells were harvested 48 hours after stimulation, resuspended in retroviral supernatant and centrifuged on retronectin (TaKaRa) coated plates. Two days after transduction, cells were harvested and cultured for 8 days in the presence of 10 ng ml-1 IL7 and IL15 (Miltenyi). At day 11 post stimulation, CAR T cells were harvested, washed using sterile PBS and diluted in PBS for intravenous injection in mice. The expressed CAR is composed of an anti-hCD70 VHH, a CD8α-based hinge, the co-stimulatory domain of 4-1BB (CD137), and the T-cell receptor-derived signaling domain CD3ζ.

NSG mice were subcutaneously injected with 2 x 10^6 SKOV3 cells. When tumors reached a size of 4-7 mm in diameter, mice were injected intravenously with PBS or 5 x 10^6 non-transfected or transfected CAR T cells with either the transfected or the nontreatment. The next day, mice were injected intraperitoneally either with PBS or with 100 µg Nivolumab (Opdivo, Bristol Myers Squibb). Tumor size was measured with a caliper.

Statistical analysis.

Differences between two datasets were assessed using one-way ANOVA and multiple comparisons were adjusted by Bonferroni corrections. Statistical significance is indicated as follow: *P<0.05, **P<0.01, ***P<0.001, ****P<0.0001.

Data availability

Source data are provided with this paper. All data supporting the findings of this study are available within the paper and its Supplementary Information. Any further related information can be provided by the corresponding author upon reasonable request.

References

36. Xiong RH, Raemdonck K, Peynshaert K, Lentacker I, De Cock I, Demeester J, et al. Comparison of Gold Nanoparticle Mediated Photoporation: Vapor Nanobubbles Outperform Direct Heating for Delivering Macromolecules in Live Cells. Acs Nano 2014, 8(6): 6288-6296.

37. Xiong RH, Joris F, Liang SY, De Rycke R, Lippens S, Demeester J, et al. Cytosolic Delivery of Nanolabels Prevents Their Asymmetric Inheritance and Enables Extended Quantitative in Vivo Cell Imaging. Nano Lett 2016, 16(10): 5975-5986.

38. Cathcart R, Schwiers E, Ames BN. Detection of Picomole Levels of Hydroperoxides Using a Fluorescent Dichlorofluorescein Assay. Anal Biochem 1983, 134(1): 111-116.

39. Lebel CP, Ischiropoulos H, Bondy SC. Evaluation of the Probe 2',7'-Dichlorofluorescin as an Indicator of Reactive Oxygen Species Formation and Oxidative Stress. Chem Res Toxicol 1992, 5(2): 227-231.

40. Bolea-Fernandez E, Balcaen L, Resano M, Vanhaecke F. Overcoming spectral overlap via inductively coupled plasma-tandem mass spectrometry (ICP-MS/MS). A tutorial review. Journal of Analytical Atomic Spectrometry 2017, 32(9): 1660-1679.

41. Encina ER, Coronado EA. Plasmon Coupling in Silver Nanosphere Pairs. J Phys Chem C 2010, 114(9): 3918-3923.

42. Encina ER, Coronado EA. On the Far Field Optical Properties of Ag-Au Nanosphere Pairs. J Phys Chem C 2010, 114(39): 16278-16284.

43. Querry MR. Optical Constants. PhD thesis, UNIVERSITY OF MISSOURI, Kansas City, Missouri, U.S., 1985.

44. Chettiar UK, Engheta N. Internal homogenization: Effective permittivity of a coated sphere. Opt Express 2012, 20(21): 22976-22986.

45. Agari Y, Ueda A. Thermal-Conductivity of Poly(Vinyl Chloride) Polycaprolactone Blends. J Polym Sci Pol Phys 1994, 32(1): 59-62.

46. Costa M, Dottori M, Sourris K, Jamshidi P, Hatzistavrou T, Davis R, et al. A method for genetic modification of human embryonic stem cells using electroporation. Nature protocols 2007, 2(4): 792-796.

47. Helledie T, Nurcombe V, Cool SM. A simple and reliable electroporation method for human bone marrow mesenchymal stem cells. Stem cells and development 2008, 17(4): 837-848.

48. Pieters T, Haenebalcke L, Hochepied T, D'Hont J, Haigh JJ, van Roy F, et al. Efficient and User-Friendly Pluripotin-based Derivation of Mouse Embryonic Stem Cells. Stem Cell Reviews and Reports 2012, 8(3): 768-778.

49. De Munter S, Van Parys A, Bral L, Ingels J, Goetgeluk G, Bonte S, et al. Rapid and Effective Generation of Nanobody Based CARs using PCR and Gibson Assembly. International journal of molecular sciences 2020, 21(3).

50. De Munter S, Ingels J, Goetgeluk G, Bonte S, Pille M, Weening K, et al. Nanobody Based Dual Specific CARs. International journal of molecular sciences 2018, 19(2).

Cover art

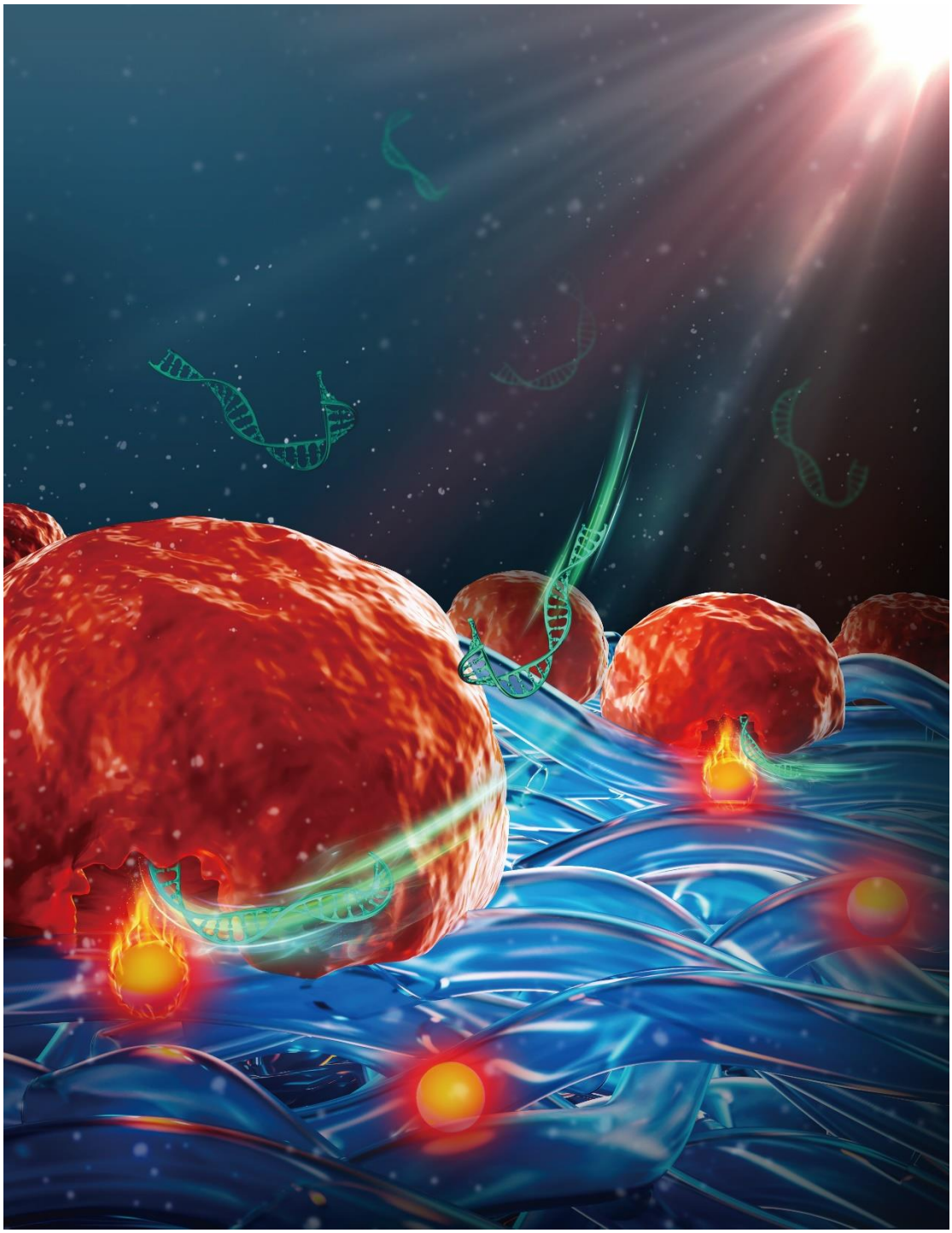

Figure 1

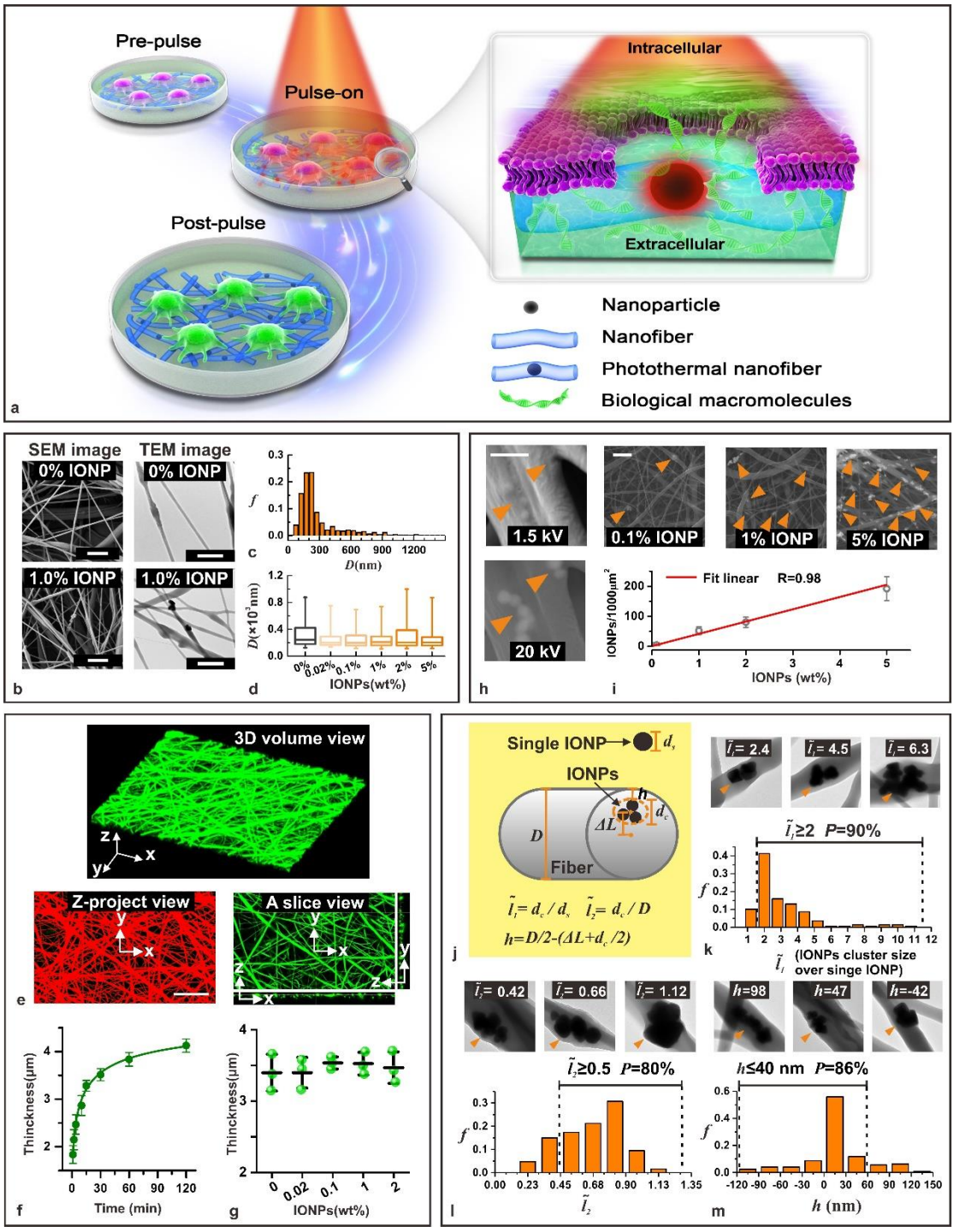
Pre-pulse
Pulse-on
Post-pulse
Intracellular
Extracellular
Nanoparticle
Nanofiber
Photothermal nanofiber
Biological macromolecules
a
SEM image
TEM image
0% IONP
1.0% IONP
b
c
d
IONPs(wt%)
1.5 kV
0.1% IONP
1% IONP
5% IONP
20 kV
h
Fit linear R=0.98
IONPs/1000μm²
IONPs (wt%)
i
3D volume view
Z-project view
A slice view
e
Thickness(μm)
Time (min)
f
g
Single IONP
IONPs
Fiber
j
k
(IONPs cluster size over singe IONP)
l
m
h (nm)

Figure 2

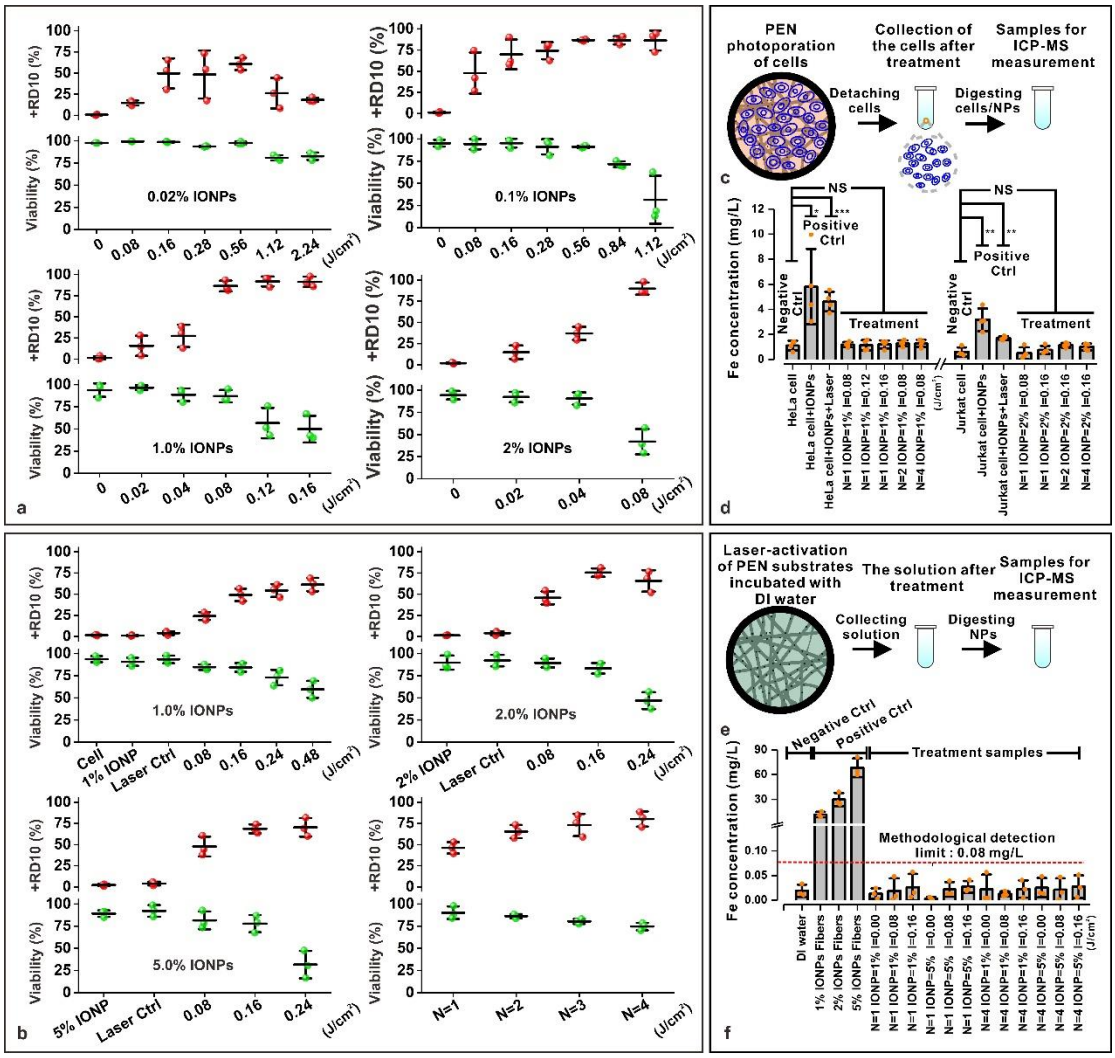
a
+RD10 (%)
Viability (%)
0.02% IONPs
0.1% IONPs
1.0% IONPs
2% IONPs
(J/cm²)
b
1.0% IONPs
2.0% IONPs
5.0% IONPs
Cell
1% IONP
2% IONP
5% IONP
Laser Ctrl
N=1
N=2
N=3
N=4
c
PEN photoporation of cells
Collection of the cells after treatment
Samples for ICP-MS measurement
Detaching cells
Digesting cells/NPs
d
Fe concentration (mg/L)
NS
Positive Ctrl
Negative Ctrl
Treatment
HeLa cell
HeLa cell+IONPs
HeLa cell+IONPs+Laser
Jurkat cell
Jurkat cell+IONPs
Jurkat cell+IONPs+Laser
e
Laser-activation of PEN substrates incubated with DI water
The solution after treatment
Collecting solution
Digesting NPs
Negative Ctrl
Positive Ctrl
Treatment samples
Methodological detection limit : 0.08 mg/L
f
DI water
1% IONPs Fibers
2% IONPs Fibers
5% IONPs Fibers

Figure 3

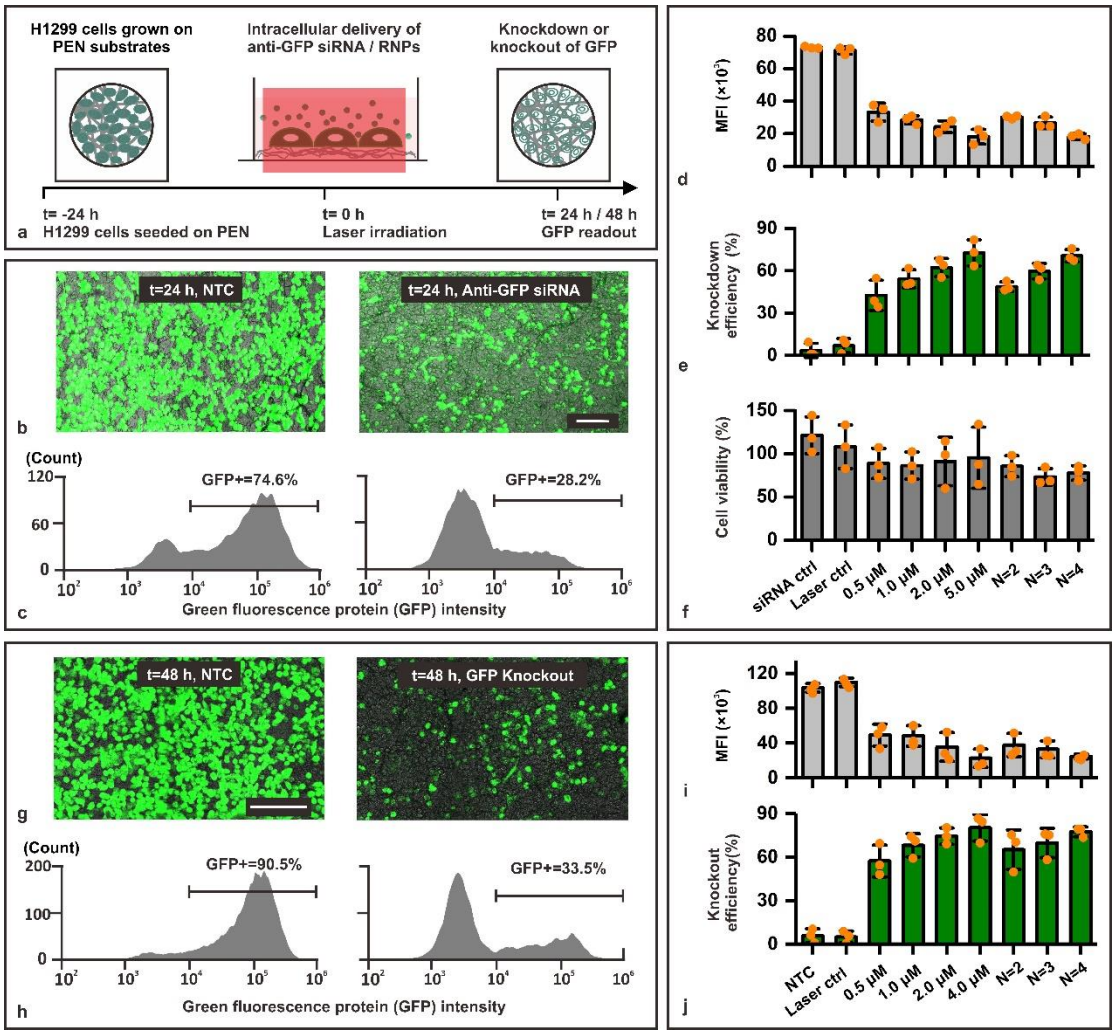
H1299 cells grown on PEN substrates
Intracellular delivery of anti-GFP siRNA / RNPs
Knockdown or knockout of GFP
t= -24 h
H1299 cells seeded on PEN
t= 0 h
Laser irradiation
t= 24 h / 48 h
GFP readout
a
t=24 h, NTC
t=24 h, Anti-GFP siRNA
b
(Count)
GFP+=74.6%
GFP+=28.2%
Green fluorescence protein (GFP) intensity
c
MFI (×10³)
d
Knockdown efficiency (%)
e
Cell viability (%)
siRNA ctrl
Laser ctrl
0.5 µM
1.0 µM
2.0 µM
5.0 µM
N=2
N=3
N=4
f
t=48 h, NTC
t=48 h, GFP Knockout
g
GFP+=90.5%
GFP+=33.5%
h
i
Knockout efficiency(%)
NTC
4.0 µM
j

Figure 4

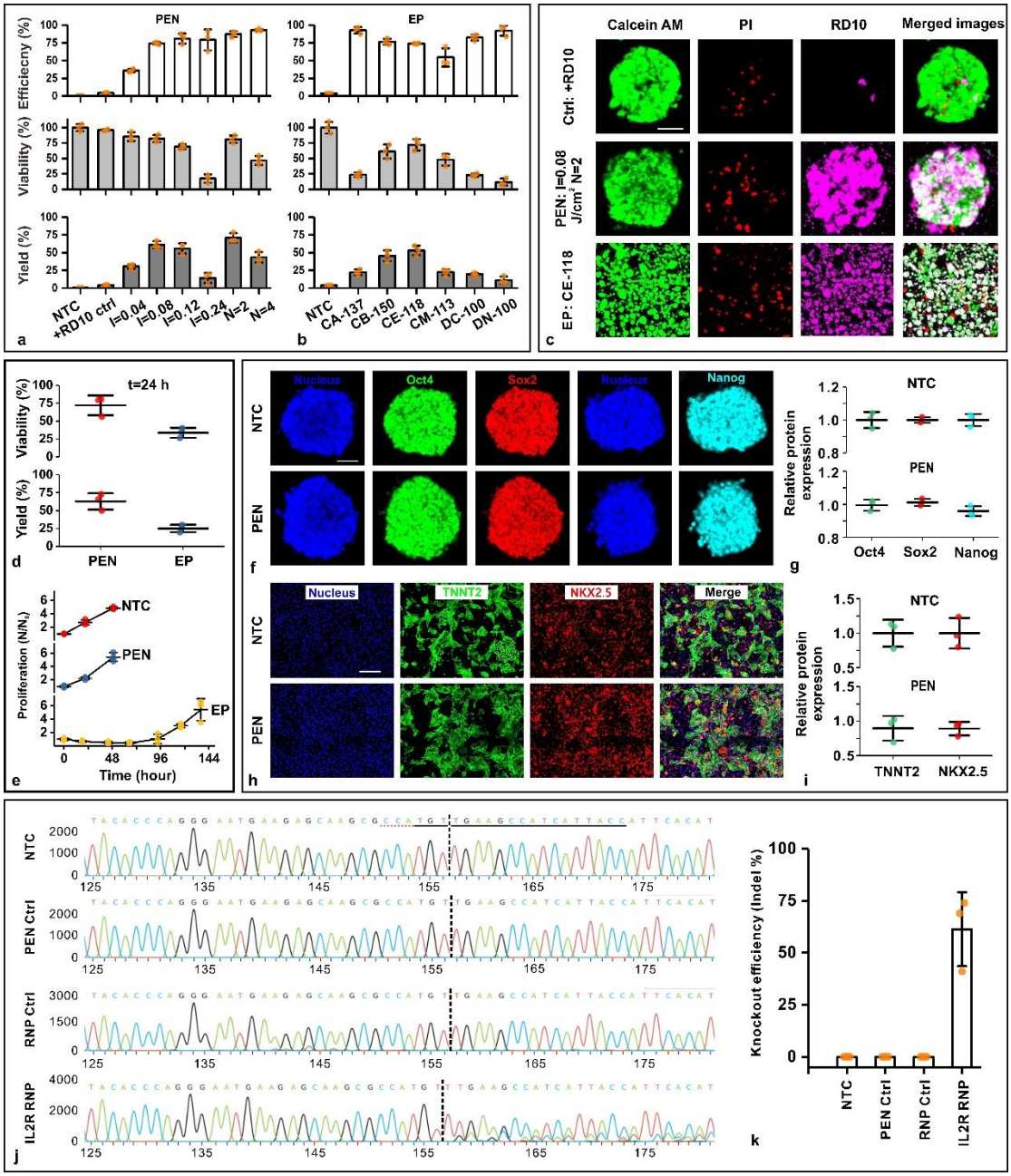
PEN
EP
Efficiecny (%)
Viability (%)
Yield (%)
NTC
+RD10 ctrl
I=0.04
I=0.08
I=0.12
I=0.24
N=2
N=4
CA-137
CB-150
CE-118
CM-113
DC-100
DN-100
a
b
Calcein AM
PI
RD10
Merged images
Ctrl: +RD10
PEN: I=0.08 J/cm² N=2
EP: CE-118
c
t=24 h
PEN
EP
d
Proliferation (N/N0)
NTC
PEN
EP
Time (hour)
e
Nucleus
Oct4
Sox2
Nanog
f
Relative protein expression
g
TNNT2
NKX2.5
Merge
h
i
NTC
PEN Ctrl
RNP Ctrl
IL2R RNP
j
Knockout efficiency (Indel %)
k

Figure 5

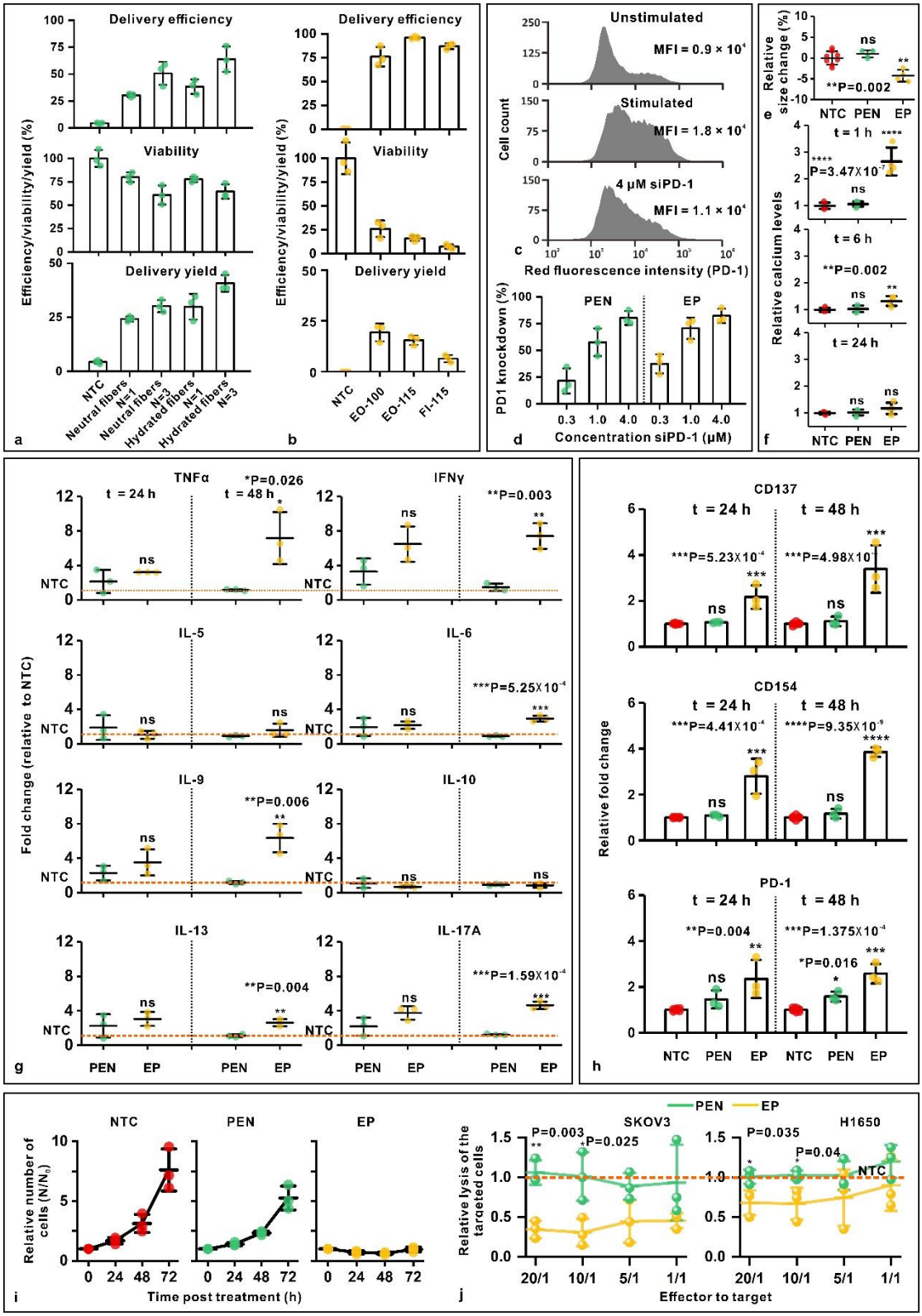
Delivery efficiency
Viability
Delivery yield
Efficiency/viability/yield (%)
NTC
Neutral fibers N=1
Neutral fibers N=3
Hydrated fibers N=1
Hydrated fibers N=3
EO-100
EO-115
FI-115
a
b
Unstimulated
MFI = 0.9 × 10⁴
Stimulated
MFI = 1.8 × 10⁴
4 μM siPD-1
MFI = 1.1 × 10⁴
Cell count
Red fluorescence intensity (PD-1)
c
PD1 knockdown (%)
PEN
EP
Concentration siPD-1 (μM)
d
Relative size change (%)
**P=0.002
e
t = 1 h
t = 6 h
t = 24 h
P=3.47X10⁻⁷
Relative calcium levels
f
TNFα
IFNγ
IL-5
IL-6
IL-9
IL-10
IL-13
IL-17A
t = 24 h
t = 48 h
*P=0.026
**P=0.003
***P=5.25X10⁻⁴
**P=0.006
**P=0.004
***P=1.59X10⁻⁴
Fold change (relative to NTC)
g
CD137
CD154
PD-1
***P=5.23X10⁻⁴
***P=4.98X10⁻⁴
***P=4.41X10⁻⁴
****P=9.35X10⁻⁹
**P=0.004
***P=1.375X10⁻⁴
*P=0.016
Relative fold change
h
Relative number of cells (N/N0)
Time post treatment (h)
i
SKOV3
H1650
P=0.003
P=0.025
P=0.035
P=0.04
Relative lysis of the targeted cells
Effector to target
20/1
10/1
5/1
1/1
j

Figure 6

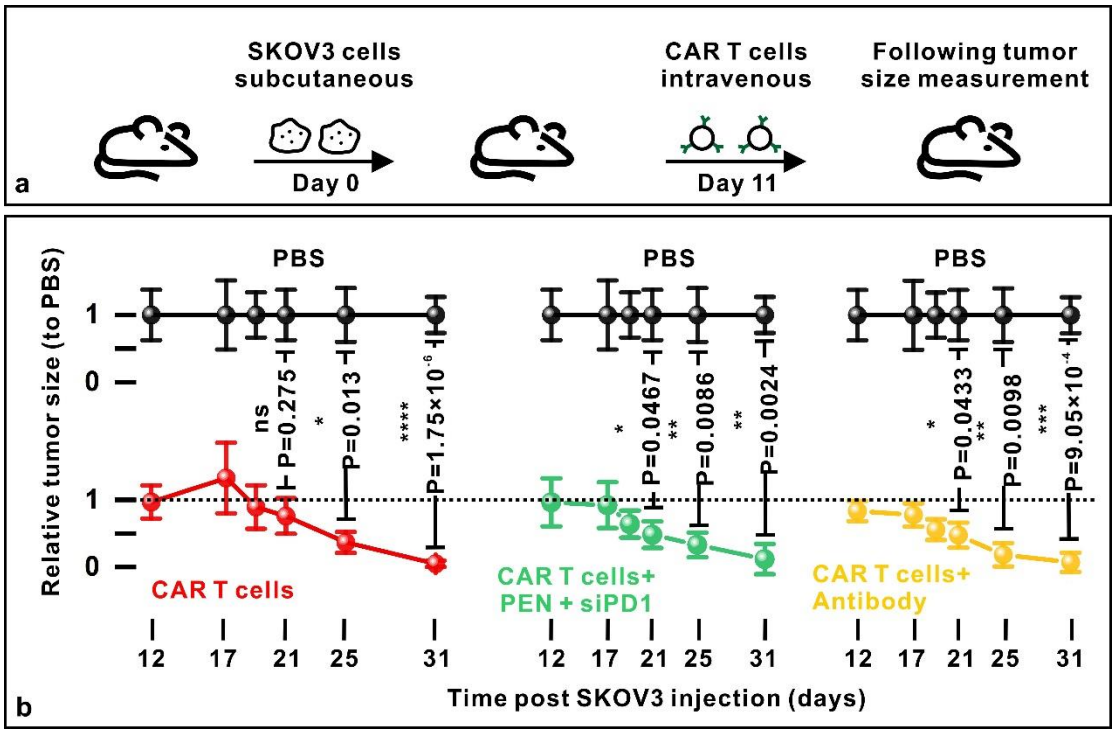
a
SKOV3 cells subcutaneous
Day 0
CAR T cells intravenous
Day 11
Following tumor size measurement
b
Relative tumor size (to PBS)
PBS
PBS
PBS
1
0
1
0
ns
P=0.275
*
P=0.013
****
P=1.75×10-6
*
P=0.0467
**
P=0.0086
**
P=0.0024
*
P=0.0433
**
P=0.0098
***
P=9.05×10-4
CAR T cells
CAR T cells+ PEN + siPD1
CAR T cells+ Antibody
12 17 21 25 31
12 17 21 25 31
12 17 21 25 31
Time post SKOV3 injection (days)